

Magnon modes for a circular two-dimensional easy-plane ferromagnet in the cone state

B. A. Ivanov

Institute of Magnetism, Ukrainian Academy of Science, Kiev, 254071, Ukraine

G. M. Wysin

Department of Physics, Kansas State University, Manhattan, Kansas 66506-2601

November 14, 2001

We calculate the magnon modes in the presence of a vortex in a circular easy-plane ferromagnet with a magnetic field perpendicular to the plane of the magnet. We also determine the range of anisotropy and magnetic field for which the two vortex branches, known as light and heavy cone state vortices, are stable. The analysis was done by combining analytical calculations in the continuum limit with numerical simulations of small discrete systems. For large enough systems the magnon modes are expressed by the S -matrix for magnon-vortex scattering. For small systems the vortex structure and consequently the magnon scattering are affected by the finite size, for which a theory designed for isotropic magnets is extended here. The presence of magnetic field in combination with easy-plane anisotropy leads to splitting of doublets both near small magnetic field and when the magnetic field is comparable to the anisotropy field. Similar doublets with splitting determined by the magnetic field may be expected in the mode spectra of small magnetic particles.

I. INTRODUCTION

In condensed matter physics vortices appear in many systems with continuously degenerate ground states, whose properties are determined by some phase-like variable ϕ , including superfluids¹ and superconductors, conventional ones² as well as high-temperature ones,³ dilute Bose-Einstein condensates,^{4,5} and some models of magnets, see Refs. 6–8. At low temperatures vortices are bound into pairs, forming a Berezinskii phase with absence of long range order, but with the presence of quasi-long-range order.⁹ The unbinding of the vortex pairs at high enough temperatures $T > T_{\text{BKT}}$ leads to the Berezinskii - Kosterlitz - Thouless phase transition, see Refs. 9–11. Vortices, free as well as bound into pairs, also play an essential role in thermal and dynamical properties of 2D magnets^{12,13} and Helium II.² In particular, translational motion of vortices leads to a central peak in dynamic correlation functions,^{12,13} which has been observed experimentally see Refs. 14 and references therein.

In this article we analyze the vortices in an easy-plane (EP) ferromagnet (FM) with a magnetic field H directed along the hard axis,¹⁵ also referred to as the *cone-state* model. There are many reasons for this interest. The initial xy-symmetry is not broken by the magnetic field; but

for magnetic field smaller than an anisotropy field H_a , the magnetization in the ground state is directed along one of the directions on the cone with the polar angle $\theta_0 \neq \pi/2$, and the FM is in so-called cone state, see 15. As $H \rightarrow H_a$, the cone angle closes, $\theta_0 \rightarrow 0$, and the Landau - Lifshitz equation for magnetization becomes equivalent to a repulsive non-linear Schrodinger equation,^{6,7} which is in fact the Gross-Pitaevsky (GP) equation used in the theory of superfluids.¹⁶ The so-called out-of-plane vortices for the cone-state model have two possible directions of the magnetization at the origin, with the “polarization”, $p = m_z(0) = \pm 1$, considered as a π_2 topological charge. This charge is in addition to the usual *vorticity* q , which has the sense of a π_1 topological charge, where q is an integer which determines the change of a phase-like variable ϕ (the condensate phase, or, for EP magnets, the azimuthal angle) along a closed contour surrounding the vortex center, $\Delta\phi = 2\pi q$. At zero magnetic field, the vortices with $p = \pm 1$ are energetically degenerate. Under the presence of $H > 0$, the two possible states of a cone-state vortex with different polarizations $p = \pm 1$ are non-equivalent, and separated by a finite energy barrier. Those with $\vec{m}(0)$ parallel to the magnetic field have a lower energy (light vortices) compared to those with $\vec{m}(0)$ antiparallel to the field (heavy vortices).¹⁵ We show that the heavy vortices lose their stability for large enough fields, and the magnetic model becomes equivalent to the GP one. The presence of a gyroscopical (Magnus) force is also a common feature for different vortices – in superfluids¹ and superconductors,² for optical vortices¹⁷, for vortices in ferromagnets see Refs. 18, 12, and for vortices in EP antiferromagnets with a magnetic field.¹⁹ For magnetic vortices the gyroforce effects are proportional to the core out-of-plane magnetization $m_z(0)$, thus it can be expected that light and heavy vortices may exhibit different gyroscopical effects.

The cone-state model also can be considered as intermediate between different models supporting vortices. Consider the deviation of the amplitude-type variable (amplitude of condensate, or out-of-plane magnetization for EP magnets), from its equilibrium value far from the vortex core. The radial dependence of this deviation is different for vortices in EP magnets and in media described by equations of GP type. The latter type (vortices in superfluidity and optics) have power law decay of this deviation far from the vortex core, in contrast with the characteristic exponential decay for vortices in

EP magnets.^{6–8} The cone-state model is intermediate between these cases, ranging from pure EP at $H = 0$ to GP as $H \rightarrow H_a$. It is natural to expect that this important difference could produce differences in dynamical properties, especially in scattering of linear excitations on a vortex and in the properties of local and quasilocal modes.

During recent years the problem of magnetic vortices for finite size magnetic particles, especially their dynamics, has become very important in connection with novel composite magnetic materials – such as magnetic dot arrays, see Refs. 20. These magnetic dots are submicron sized islands made from soft magnetic materials on a non-magnetic substrate. They are important from a practical standpoint (high-density magnetic storage) and are interesting as fundamentally new objects in the basic physics of magnetism. The distribution of magnetization in such a dot is quite nontrivial: when the dot size R is above the critical value R_{cr} , an inhomogeneous state with an out-of-plane magnetic vortex occurs, stable due to competition between exchange and dipole interactions.²¹ This vortex state has been experimentally observed for disk-shaped magnetic dots with the diameter $2R = 200 - 800$ nm and thickness $L = 20 - 60$ nm.²² It is expected that these non-uniform states will drastically change the dynamic and static properties of a dot in comparison with a uniformly magnetized magnetic disk. The cone state vortices are also important for the description of real systems of sub-micron magnetic dots, because the magnetic dipole interaction of dots in the lattice produces a magnetic field perpendicular to the dots' plane. This field could be either parallel or antiparallel to the magnetization of the core of the vortex of the dot, implying the presence of both light and heavy cone-state vortices, respectively.

To construct an adequate description of the vortex ensemble and vortex contributions to the dynamical response functions, it is necessary to investigate the dynamical properties of single vortices, including the translational motion as well as the properties of local and quasilocal modes (internal modes) on the vortex. The investigation of vortex dynamics (translational and internal) has been carried out using different methods – numerically, for discrete models, mainly for circular samples cut from large lattice systems, see Refs. 23, 24, and for continuum models as well, both analytically, see Refs. 25–27 and numerically, see Refs. 28, 29. A better understanding of this the problem of vortex dynamics in the finite-size circular magnets was developed in Refs. 30, 29. These problems are deeply connected with the problem of scattering of linear excitations by a vortex, which we investigate in detail here. For example, knowledge of the S-matrix for vortex-magnon scattering gives the possibility to describe the results of numerical simulations of the motion of the magnetic vortex, and to verify a non-Newtonian dynamical equation for the vortex center coordinate, see Ref. 30.

Due to the above reasons, in this article we concentrate

on developing the theory for scattering of magnons by a cone-state vortex, determining scattering data for both light and heavy vortices. We find particularly interesting features, including a strongly magnetic-field-dependent splitting of doubly degenerate modes. As part of our calculations, we determined the stable light and heavy vortex structures as functions of magnetic field. The main body of the article is organized as follows. In Sec. II we present the model, and discuss its ground state, free magnon excitations, and the cone-phase out-of-plane vortices. The stability of these vortices is investigated numerically and through a variational calculation. In Sec. III we describe the numerical calculation of modes on a vortex, and also give the basic theory for magnon modes on a vortex, as derived from the Landau-Lifshitz dynamical equations. In Sec. IV we focus on analysis and presentation of results for *finite-radius* circular magnetic particles in the cone state, where finite size effects play a strong role. The main conclusions of our work are summarized in Sec. V.

II. THE MODEL, GROUND STATE AND EXCITATIONS.

We consider the classical two-dimensional (2D) model of a Heisenberg ferromagnet (FM) in the presence of an external magnetic field H , with the Hamiltonian

$$\mathcal{H} = -J \sum_{(\vec{n}, \vec{n}')} \{ \vec{S}_{\vec{n}} \cdot \vec{S}_{\vec{n}'} - (1 - \lambda) S_{\vec{n}}^z S_{\vec{n}'}^z \} - g\mu_B H \sum_{\vec{n}} S_{\vec{n}}^z. \quad (1)$$

Here $J > 0$ is the exchange integral, and $0 \leq \lambda < 1$ describes easy-plane anisotropy with (xy) as the easy plane. The spins \vec{S} are classical vectors on a square lattice with the lattice constant a . (\vec{n}, \vec{n}') denotes nearest-neighbor lattice sites, counting each bound only once. The magnetic field H is directed along the hard axis, because only in this case is the initial xy -symmetry not broken by the magnetic field; g is Lande factor, μ_B is the Bohr magneton. Our main interest lies in the small anisotropy case, which corresponds to $1 - \lambda \ll 1$, for which a continuum limit analysis is valid.

A continuum limit for the FM model can be derived from (1) in the usual way, defining the unit vector of magnetization as a function of continuous variables \vec{r} and t : $\vec{m}(\vec{r}, t) = \vec{S}_{\vec{n}}(t)/S$. The dynamical equation for \vec{m} has the form of the well-known Landau-Lifshitz equation, see Refs. 6, 7. In usual angular variables [$m_x + im_y = \sin \theta \exp(i\phi)$, $m_z = \cos \theta$], its form is dictated by the continuum energy functional $E[\theta, \phi]$, according to

$$S \sin \theta \frac{\partial \phi}{\partial t} = \frac{\delta E}{\delta \theta}, \quad S \sin \theta \frac{\partial \theta}{\partial t} = -\frac{\delta E}{\delta \phi}. \quad (2)$$

For the model (1), in the lowest approximation with small parameter $1-\lambda$ and small gradients of magnetization, the energy functional can be presented in the form

$$E[\theta, \phi] = JS^2 \int d^2r \left[(\nabla\theta)^2 + (\nabla\phi)^2 \sin^2\theta + \frac{1}{r_v^2} (\cos\theta - h)^2 \right]. \quad (3)$$

Here we introduced the characteristic length scale, r_v , which gives the vortex core size at $H = 0$, and the dimensionless magnetic field, h , normalized by the anisotropy field H_a , which are defined by

$$r_v = \frac{a}{2} \sqrt{\frac{\lambda}{1-\lambda}}, \quad h = \frac{H}{H_a}, \quad g\mu_B H_a = 4JS(1-\lambda). \quad (4)$$

For a material with a typical exchange interaction $J \approx 10$ K, $g = 2$, and one-percent anisotropy, $\lambda \approx 0.99$, this gives an anisotropy field of $H_a \approx 0.3$ Tesla and a vortex core size $r_v \approx 5a$, where a is the lattice constant.

A. Ground State

For small fields $h < 1$ (valid for small laboratory fields and real materials), the minimization of the energy (3) shows that the ground state is the so-called *cone state*, in which the asymptotic value of $\theta = \theta_\infty \neq \pi/2$, is determined by the normalized magnetic field strength,

$$\cos\theta_\infty = h, \quad (5)$$

and the value of ϕ is arbitrary; see Refs. 6, 7 for details. In this state the symmetry of the ground state is lower than that of the model. For zero magnetic field, $\theta_\infty = \pi/2$, and we have a usual easy plane ferromagnet. For large enough fields, $h \geq 1$, the collinear phase with the magnetization parallel to the magnetic field ($\theta = 0$) is realized.

The dynamical equations for this model can be written as

$$\nabla^2\theta - (\nabla\phi)^2 \sin\theta \cos\theta + \frac{1}{r_v^2} \sin\theta (\cos\theta - h) = + \frac{\sin\theta}{c_0 r_v} \frac{\partial\phi}{\partial t} \quad (6a)$$

$$\nabla(\sin^2\theta \nabla\phi) = - \frac{\sin\theta}{c_0 r_v} \frac{\partial\theta}{\partial t} \quad (6b)$$

where $c_0 = 2JSa\sqrt{1-\lambda}$ is the magnon speed at $H = 0$.

Note that the equations (3) and (6) arise in the long-wave approximation ($a|\nabla\vec{m}| \ll 1$) not only for the model we are considering here, but for a set of discrete models, for example, on different uniaxial lattices, like triangular and hexagonal. Merely the expressions for c and r_v , defined through the microscopic parameters J and λ , change. We should point out, however, that the terms describing the inhomogeneous exchange interaction for the

model (1) read $(\lambda \sin^2\theta + \cos^2\theta)(\nabla\theta)^2 + (\nabla\phi)^2 \sin^2\theta$. We work with the more symmetric form of the energy displayed in (3), for the following reasons. First, for small anisotropy ($\lambda \simeq 1$), the theta-dependence of the multiplier before $(\nabla\theta)^2$ is unimportant. Second, and more essential, Eq. (3) holds for various models, for example, for FMs on different kinds of lattices and FMs with additional single-ion anisotropy. For all of these models, with small enough anisotropy ($r_v \gg a$), the energy (3) is universal in the long wavelength approximation, instead of having different non-symmetrical generalizations like the one presented above.

B. Free Magnons

For the homogeneous ground state (all spins are parallel and confined to one of the directions on the cone $\cos\theta = h$) the 2D model has well-known magnon excitations with the gapless dispersion law

$$\omega = k \cdot c(h) [1 + k^2 r_v^2(h)]^{1/2} \quad (7)$$

where $k = |\vec{k}|$ and \vec{k} is the magnon wave vector, and the parameters are

$$c(h) = c_0 \sqrt{1-h^2}, \quad (8a)$$

$$r_v(h) = \frac{a}{2} \sqrt{\frac{h^2(1-\lambda) + \lambda}{(1-\lambda)(1-h^2)}} \simeq \frac{r_v}{\sqrt{1-h^2}}. \quad (8b)$$

These have the same physical sense for a FM in the presence of the magnetic field as (4) and (6) for $H = 0$. It is important to note that the presence of the magnetic field increases the value of r_v and makes the region of applicability of the continuum model wider. For example, even for the XY-model, which has extremely high anisotropy, the value of $r_v(h)$ for nonzero fields is finite, and becomes more than the lattice constant for $H \cong H_a$. On the other hand, for some type of vortices (so-called heavy ones, discussed below) the simplest continuum model (3) fails, and the next powers of gradients of magnetization have to be taken into account.

C. Cone-Phase Out-of-Plane Vortices

For the weak anisotropy considered here ($\lambda \simeq 1$), or for large enough magnetic field, the stable vortex excitations have a nonzero out-of-plane (S^z) component. These out-of-plane (OP) vortices are described by the formulas

$$\theta = \theta_0(r) \quad , \quad \phi = q\chi + \phi_0 \quad (9)$$

where r and χ are polar coordinates in the FM's easy plane, and $q = \pm 1, \pm 2, \dots$ is the π_1 -topological charge

(vorticity). The function $\theta_0(r)$ is the solution of a non-linear ordinary differential equation,^{6,7} with the natural boundary conditions, $\sin\theta_0 \rightarrow 0$ at $r \rightarrow 0$, giving the absence of a singularity at the origin, and $\cos\theta_\infty = h$ far from the vortex. The value of $\cos\theta_0(0) = \pm 1$ determines two possible states of the vortex with given q . For the case $H = 0$, the vortices with $p = \cos\theta_0(0) = \pm 1$ correspond to the mapping of the FM's plane onto the upper and lower half-spheres of the sphere $\vec{m}^2 = 1$. Thus, the value of $p = \cos\theta_0(0)$ can be considered as a π_2 topological charge, the so-called polarization. For zero field the vortices with $p = \pm 1$ have the same energies, but can be transformed into each other only by the creation of discontinuities of the magnetization field (2D analog of hedgehog-like singular points, which is common to in-plane vortices), see Ref. 31. The energy barrier that has to be overcome to reverse the vortex polarization is finite, in contrast with the infinite energy barrier to change the π_1 topological charge vorticity. For the case $h \neq 0$, the vortices with $\vec{m}(0)$ parallel to the magnetic field have a lower energy (light vortices) compared to the vortices with $\vec{m}(0)$ antiparallel to the field (heavy vortices). Alternatively, we find it is more convenient to always put $\cos\theta_0(0) = +1$, and then allow both positive and negative values of the magnetic field. Then the case $h > 0$ corresponds to light vortices, and $h < 0$ corresponds to heavy ones.

1. Light and Heavy Vortices: Theory

Both light and heavy vortices can be described in continuum theory. For the simplest model (3), their structure can easily be found by numerical integration of the second order differential equation for $\theta_0(r)$, which for this model reads¹⁵

$$\frac{d^2\theta_0}{dx^2} + \frac{1}{x} \frac{d\theta_0}{dx} - \frac{q^2}{x^2} \sin\theta_0 \cos\theta_0 + \sin\theta_0 (\cos\theta_0 - h) = 0, \quad (10)$$

where $x = r/r_v$, with the boundary conditions

$$\cos\theta_0(0) = 1, \quad \cos\theta_0(\infty) = h, \quad (11)$$

Only the case $q^2 = 1$ will be discussed here. Numerical integration (also see following section) gives solutions for all values of the magnetic fields $-1 < h < 1$, where $h > 0$ corresponds to the light vortices, and $h < 0$ to the heavy ones.¹⁵ Let us discuss briefly the vortex structure. At $x \rightarrow 0$ the value of $\theta \rightarrow Cx$, just as for the case $h = 0$, but with the constant C depending strongly on h . Far from the vortex, the asymptotics change drastically and follow the power law, $\cos\theta_0 = h + h/x^2$, instead of the exponential one, $\cos\theta_0 \sim \exp(-x)$ for $h = 0$. This power law dependence is valid for both signs of the magnetic field, e.g. for both light and heavy vortices, at the values $x \gg \max\{1, h/\sqrt{1-h^2}\}$. The power law decay is a typical property of vortices for different media,

like those in hydrodynamics and superfluidity, whereas the exponential dependence can be considered an exception. As we will see later, the appearance of power law asymptotics produces very important differences in the dynamical properties of the magnetic vortices at $h = 0$ and $h \neq 0$.

For light vortices, with growing magnetic field the amplitude of the function $\cos\theta_0(r)$ decreases and the region of its localization $\Delta r \sim r_v(h)$ increases. On the other hand, even for values of $(1-\lambda)$ significantly different from zero, including up to $\lambda = 0$ (*XY*-model), the continuum approximation can be valid at large positive values of $h \simeq 1$. For example, for $\lambda = 0$, we have $r_v(h) = 3.5a$ at $H = 0.99H_a$ and $r_v(h) = 11.2a$ at $H = 0.999H_a$. For finite systems, even for large system radii $R \gg r_v$, the light vortex core width $r_v(h)$ can become larger than the system radius R at large enough fields, $(1-h) < (r_v/R)^2$. In this case some special approximations based on an isotropic model must be considered, and are presented below.

For heavy vortices the situation is opposite: at $h \rightarrow -1$ the function $\cos\theta_0(r)$ becomes very sharp near the origin and the region of the vortex core becomes very narrow, even less than a lattice constant, see Ref. 15. Thus, if one starts with small values of the anisotropy parameter $(1-\lambda)$, the continuum approximation fails at values of h near -1 . Note that this behavior is not connected with the value of $r_v(h)$, which becomes large for positive and negative fields. As was shown numerically in Ref. 15, for large negative fields there are two different scales in the vortex structure: the large value $r_v(h)$ determines the asymptotics far from the vortex core, while the vortex core width can be much smaller. This feature manifests itself in the properties of the vortices in the finite sized discrete model.

2. Light and Heavy Vortices: Numerical Relaxation and Discussion

An alternative way to construct the vortex states is the direct energy minimization of the discrete model (1), see Ref. 28. Starting from a very rough approximation for the vortex spin directions on a circular square lattice system, with cone phase boundary conditions, $\cos\theta(R) = h$, we relaxed the configuration with a method that directly seeks the energy minimum for the given field h . We started from zero field, relaxed the configuration, then used that configuration as the initial state for the relaxation at the next field strength, and so on, thereby determining the vortex structure for a sequence of positive or negative field strengths.

Results for the spin configuration $\cos\theta_0(r)$ for light vortices are shown in Fig. 1. The vortex core width $w(h)$ increases with applied field; the vortex becomes smoother with increasing field strength. For λ close to 1, the results are universal functions of $r/r_v(0)$, as expected where the

continuum limit applies. As λ is allowed to deviate more from 1, minor differences from the continuum results appear, especially in the core region of the vortex. In general, however, discreteness of the lattice has a minimal effect on the structure of the light vortices.

For heavy vortices, the lattice plays a stronger role, especially as λ deviates from 1. First, for $\lambda = 0.999$, where $r_v(0) = 15.8a$, discreteness effects are weak. In Fig. 2, the resulting spin configurations are shown, where it is seen that the vortex core width $w(h)$ decreases strongly at negative fields. When $w(h)$ gets sufficiently small, the heavy vortex becomes unstable towards conversion to a light vortex, as seen at $h = -0.9$, where $\cos\theta_0(0) = -1$ resulted (the core spins reversed during the relaxation, because there is no topological constraint on them in a discrete system). This discrete effect is stronger at $\lambda = 0.96$, as seen in Fig. 3, where the conversion to light vortices occurs around $h \approx -0.4$. Certainly this is because the value $r_v(0) = 2.45a$ is much smaller in this case, so the heavy vortex destabilizes at a much weaker field. Generally, the conversion to light vortices occurs when the field-dependent vortex core width becomes smaller than $r_v(0)$, but is still larger than the lattice constant. We explain this heavy vortex instability effect below.

In Fig. 4 we also show the total vortex energy E minus the ground state energy per site in the cone state, E_c , which has $\cos\theta(r) = h$ everywhere. By this definition, there is a logarithmic dependence of the vortex energy on the system radius R . In Figure 4 the curves at different λ were all calculated using the same system radius, $R = 50a$. The curves are of finite extent on the negative h -axis, due to the instability of the heavy vortices there at some critical value of the magnetic field, $h = h_c < 0$. This instability never appears in a continuum model.

Thus, for heavy vortices, we have a qualitative discrepancy between the results of continuum and discrete models. For the continuum model, heavy vortices are present for all fields $-1 < h < 0$; for the discrete model, some critical field appears. Note that the instability field h_c is not too close to -1 even for small anisotropies, like $\lambda = 0.999$. We have found that to describe this interesting feature, it is necessary to go beyond the simplest continuum model (3), and take into account the higher space derivative terms. In principle, there is no problem to write down equations to include such terms, but it is not customary to do so for the 3D case. The reason is as follows: these terms have the next higher powers of the smallest scale of the problem, the lattice constant a . If the characteristic width of the soliton is much larger than a , these terms are small and unimportant corrections. If this width becomes comparable with a , it seems senseless to limit oneself to accounting for only one more term, all the terms might give comparable contributions. As we will see, for 2D this is not the case, and the contributions from derivatives higher than four are negligible. This feature has the same origin as the observation mentioned above, that the vortex core width at the instability point, $w_c \equiv w(h_c)$, lies between two characteristic values, $r_v(0)$

and a .

3. Heavy vortices: discrete lattice instability

To investigate the vortex structure and stability with fourth derivative terms, it is enough to expand the Hamiltonian of discrete model (1) up to higher powers of $\nabla\vec{m}$, so that an additional term ΔE appears in the energy,

$$\Delta E = -\frac{Ja^2}{24} \int dx dy \left\{ \left(\frac{\partial^2 \vec{S}}{\partial x^2} \right)^2 + \left(\frac{\partial^2 \vec{S}}{\partial y^2} \right)^2 - 2 \frac{\partial^2}{\partial x^2} \left(\frac{\partial \vec{S}}{\partial x} \right)^2 - 2 \frac{\partial^2}{\partial y^2} \left(\frac{\partial \vec{S}}{\partial y} \right)^2 \right\}. \quad (12)$$

Note that in this expression, valid for a square lattice, we kept the full derivative terms. They could be important if the functions with jumps of derivatives [like (17) below] are used. In principle, one could rewrite this term in angular variables, and construct the corresponding Lagrange equation for this energy functional and find the solution describing the vortex. But realization of this program is a much more complicated task than the vortex description for the simplest model (3) with $\Delta E = 0$. This is because, first and foremost, the terms with higher derivatives produce fourth-order anisotropy in coordinate space, and the simple ansatz (9) becomes invalid. Then a general solution like $\theta = \theta(r, \chi)$, $\phi = \phi(r, \chi)$ must be considered. Unfortunately, there are no general methods to solve such problems, and an analysis may be carried out only numerically with the use of different variational methods.³²

Thus, the exact solution of the set of two partial differential equations for these functions cannot be found. In order to simplify the problem, suppose that the fourth-order anisotropy is weak, and $\phi(r, \chi)$ can be approximated by the more symmetrical form (9). Using this approximation, we arrive at some functional involving the angle $\theta(r)$. Minimization of this functional gives us a fourth order ordinary differential equation for $\theta(r)$. But even with this approximation the problem is still challenging. Note that the solutions for the second order equation (10), as for any dynamical problem with one degree of freedom, can easily be presented on the phase plane. The separatrix solution can easily be constructed numerically by use of a usual one-parameter shooting method. The fourth order equation, however, is equivalent to a much more complicated dynamical problem with *two* degrees of freedom. Its solutions are trajectories in four dimensional phase space, which could manifest strange attractors, quasi-stochastic behavior and other complex features. To find the separatrix solution, (it is just an approximate solution of the original partial differential equation) one needs to use a three-parameter shooting scheme, and we do not know any examples of its numerical realization.

In this situation we have used a simpler qualitative analysis. Let the vortex structure be described by some universal function $\theta = f(r/W)$, with a characteristic vortex core size W . This immediately gives the vortex energy as a function of W in the form

$$\frac{E}{\pi JS^2} = \sin^2 \theta_0 \ln \frac{R}{W} - \frac{1}{2} \left(\frac{a}{W} \right)^2 A(h) + \frac{1}{2} (1 - \lambda) \left(\frac{W}{a} \right)^2 B(h) + C(h), \quad (13)$$

where $A(h)$, $B(h)$, $C(h)$, are determined by the function $f(x)$, and depend only on the magnetic field, or, equivalently, on the ground state value of the polar angle θ_0 . Minimization of this energy with respect to W gives a biquadratic equation for the vortex core width W , whose solution,

$$W^2 = \frac{a^2}{2B(1-\lambda)} \left[\sin^2 \theta_0 + \sqrt{\sin^4 \theta_0 - 4(1-\lambda)AB} \right], \quad (14)$$

depends primarily on the functions $A(h)$, $B(h)$, which are smooth and nonzero for all $-1 < h < 0$, in the region of interest, $\pi/2 < \theta_0 < \pi$. Then the features mentioned above (heavy vortex instability) immediately become obvious. It is found that the equation for W has a solution only for h above a (negative) critical value, $h_c < 0$. If $h < h_c$, where the critical value of magnetic field h_c is the solution of transcendental equation,

$$(1 - h_c^2)^2 = 4(1 - \lambda)A(h_c)B(h_c), \quad (15)$$

the minimum is absent and the heavy vortex is unstable. At the point of instability the value of the vortex core width W_c can be written as

$$W_c = \frac{a}{\sqrt{2B(h_c)}} \frac{\sqrt{1 - h_c^2}}{\sqrt{1 - \lambda}} = a \cdot \left[\frac{A(h_c)}{(1 - \lambda)B(h_c)} \right]^{1/4}. \quad (16)$$

Thus, the vortex core width $W(h)$ near the instability point h_c has the order of magnitude $\sqrt{ar_v}$, and $a \ll W(h_c) \ll r_v$. $W(h_c)$ is smaller than the characteristic length r_v , but at the same time, much larger than the lattice constant a . This means that (i) the generalized macroscopic approximation including fourth derivative terms is valid down to the critical value of magnetic field, $h_c < 0$; (ii) terms in the energy with space derivatives higher than four are unimportant. So the estimate given here is self-consistent.

Two more results are clearly seen from Eq. (15): (i) the critical value $1 - h_c$ is proportional to $\sqrt{1 - \lambda}$ for extremely small anisotropies, namely, $1 - |h_c| \rightarrow \sqrt{(1 - \lambda)A(-1)B(-1)}$ as $\lambda \rightarrow 1$, and (ii) heavy vortices could be absent for high enough anisotropy. If the value of $4A(0)B(0)$ is larger than 1 (as we will see, it is the case), for $\lambda = \lambda_c$, where $1 - \lambda_c = 1/[4A(0)B(0)]$, the value of h_c becomes equal to zero, and for $\lambda < \lambda_c$, the

concept of heavy vortices loses sense. These features are in good agreement with our numerical simulation data, see Figs. 2 – 4.

To make concrete estimates of h_c and λ_c , and test the above predictions, we choose a specific one-parameter variational function for the heavy vortex,

$$\theta(r) = \theta_0 \frac{r}{W}, \quad r \leq W, \quad (17a)$$

$$\theta(r) = \theta_0 \quad r > W, \quad (17b)$$

where the variational parameter W can be considered as the vortex core size.

Due to general properties of variational methods, if the solutions of such equations are known with the accuracy $\delta \ll 1$, the energy calculated using this approximate solution gives the vortex energy with the accuracy δ^2 . In particular, the corrections linear and quadratic in these small corrections have the same order of magnitude. Thus we believe that using even the simple function (17) could explain, at least semi-qualitatively, the features mentioned above (i.e., unstable heavy vortices) and absent for the simplest continuum model (3).

Inserting this trial function into the energy [including (3) and the fourth order terms of Eq. (12)], after long but simple algebra we arrive at a concrete form for the coefficients A, B, C . It is convenient to write them in terms of θ_0 , related to h via Eq. (11), as

$$A(\theta_0) = \frac{\sin^2 \theta_0}{3} + \frac{\theta_0^4}{16} - \frac{3\theta_0^2}{8} + \frac{\theta_0}{4} \sin \theta_0 \cos \theta_0 + \frac{5\theta_0^2}{8} \int_0^{\theta_0} \frac{dx}{x} \sin^2 x \quad (18a)$$

$$B(\theta_0) = \frac{2}{\theta_0^2} \left[(1 + 2 \cos^2 \theta_0) \theta_0^2 - 6\theta_0 \sin \theta_0 \cos \theta_0 - 7 \cos^2 \theta_0 + 8 \cos \theta_0 - 1 \right]. \quad (18b)$$

$$C(\theta_0) = -\frac{R^2 h^2}{2r_v^2} + (\theta_0)^2/2 + \int_0^{\theta_0} \frac{dx}{x} \sin^2 x. \quad (18c)$$

Here A is presented for $\lambda = 1$; there are minor corrections as λ deviates from 1. $C(\theta_0)$ is useful for absolute comparison of the variational theory with simulations. The first term in C is the ground state energy of the cone state; the other terms are due to the presence of the vortex.

Calculation of the integrals in A and then solving Eq. (15) can only be done numerically, and gives us the possibility to describe the dependence $h_c(\lambda)$. This theoretical dependence is plotted and compared with estimates of h_c from numerical simulation of heavy vortices in Fig. 5. The theory is in good agreement with the critical field as found for vortices on a lattice, which is rather surprising when we consider that we used a rather

rough trial function. The simulation data does not fit to any simple power law over the range of anisotropy studied, but as $\lambda \rightarrow 1$, follows approximately the form, $(1 - |h_c|) \approx 22(1 - \lambda)^{0.34}$.

For extremely small anisotropy $(1 - \lambda) \ll 1$, then $1 - |h_c| \ll 1$, and one can use the limiting values: $A(h \rightarrow -1) \approx 9.9053$, $B(h \rightarrow -1) \approx 2.7577$. These result in the estimated asymptotic dependence, $(1 - |h_c|)_{\text{theory}} \approx 5.23\sqrt{1 - \lambda}$, whereas the numerical data give a slightly different power and prefactor, as mentioned above. The discrepancy probably can be attributed to the fact that in the numerical simulations, the lowest anisotropy values used, $(1 - \lambda) \approx 10^{-3}$, are not far enough into the asymptotic regime, see inset of Fig. 5. Similarly, using the limiting values as $h \rightarrow 0$, we estimated the limiting value of the anisotropy constant, $(\lambda_c)_{\text{theory}} \approx 0.8$, below which heavy vortices should be absent. In the numerical solution, we found stable heavy vortices down to $\lambda \approx 0.72$ and perhaps slightly lower, which is actually out to the anisotropy limit where all vortices become in-plane (where no heavy/light vortex distinction is possible). From these results using the linearized ansatz for the vortex structure, we can conclude that both stability limits are essentially caused by discreteness effects due to the lattice, which are taken into account to leading order by the fourth order derivative terms.

III. MAGNON-VORTEX SCATTERING AND NORMAL MODES

Once the static cone-phase vortex structure has been found, we are interested in the presence of magnons on top of that structure. As mentioned in the Introduction, the presence of the H-field leads to interesting new features in the magnon spectrum, in particular, it induces a large splitting of states that are barely split at zero field. In this section we first present the numerical calculation of the vortex-magnon modes, followed by a theoretical analysis of the doublet splitting and the other new features.

A. Numerical calculation of the modes

We consider a semiclassical calculation of the magnon modes on top of a vortex in a finite circular system of radius R , with the spins on an underlying square lattice. If $\phi_{\mathbf{n}}^0$ and $\theta_{\mathbf{n}}^0$ represent the vortex structure on lattice sites \mathbf{n} , then we assume a perturbation to this structure in the form,

$$\phi_{\mathbf{n}} = \phi_{\mathbf{n}}^0 + \varphi_{\mathbf{n}} \quad , \quad \theta_{\mathbf{n}} = \theta_{\mathbf{n}}^0 + \vartheta_{\mathbf{n}}, \quad (19)$$

where the equations of motion need to be linearized in terms of the small fluctuations, $\varphi_{\mathbf{n}}$ and $\vartheta_{\mathbf{n}}$.

In Ref. 24, a formalism and set of coordinates were described for finding magnon-vortex scattering on lattice

systems. For determination of the modes numerically, local Cartesian coordinates for the spins are more convenient than spherical coordinates. The unperturbed spins of the static vortex structure, $\mathbf{S}_{\mathbf{n}}^0$, are considered to define *local* quantization axes $\tilde{z}_{\mathbf{n}}$, different at every site, specifically,

$$\mathbf{S}_{\mathbf{n}}^0 = S\tilde{z}_{\mathbf{n}}. \quad (20)$$

Then the perturbation of this structure involves fluctuations orthogonal to the $\tilde{z}_{\mathbf{n}}$ -axis, along two other local Cartesian axes $\tilde{x}_{\mathbf{n}}$ and $\tilde{y}_{\mathbf{n}}$. The $\tilde{x}_{\mathbf{n}}$ -axis is taken to be along the direction defined by the cross product $\tilde{x}_{\mathbf{n}} = z_{\mathbf{n}} \times \tilde{z}_{\mathbf{n}}$, which is within the original xy (easy) plane. The last axis of the local coordinates for a site is $\tilde{y}_{\mathbf{n}} = \tilde{z}_{\mathbf{n}} \times \tilde{x}_{\mathbf{n}}$. Then the perturbation of the static vortex structure can be expressed in terms of its spin components along the new local axes:

$$\mathbf{S}_{\mathbf{n}} = \mathbf{S}_{\mathbf{n}}^0 + S_{\mathbf{n}}^{\tilde{x}} \tilde{x}_{\mathbf{n}} + S_{\mathbf{n}}^{\tilde{y}} \tilde{y}_{\mathbf{n}}. \quad (21)$$

A short calculation shows that these are related to the angular perturbation coordinates by

$$S_{\mathbf{n}}^{\tilde{x}} = S\varphi_{\mathbf{n}} \sin \theta_{\mathbf{n}}^0, \quad S_{\mathbf{n}}^{\tilde{y}} = S\vartheta_{\mathbf{n}}. \quad (22)$$

The variables $S_{\mathbf{n}}^{\tilde{x}}$ and $\varphi_{\mathbf{n}}$ relate to purely in-plane spin motions, while $S_{\mathbf{n}}^{\tilde{y}}$ and $\vartheta_{\mathbf{n}}$ measure the change in out-of-easy-plane tilting, relative to the local spin direction in the unperturbed vortex.

For circular systems of radius R , we used a Gauss-Seidel relaxation scheme³³ to calculate some of the lowest magnon modes with either a single light or heavy vortex present in the system. We considered different values of λ close to 1, and the applied field h was allowed to vary between some (negative) lower critical limit h_c and 1. Although the continuum limit would be better represented by using λ very close to 1, this would result in the vortex radius $r_v(0)$ easily exceeding the system size that can be solved numerically. Therefore, we show some results with $\lambda = 0.96$, where $r_v(0) \approx 2.45a$, so even for “very light” vortices with $h = 0.99$, the field dependent core radius [Eq. (4)] is $r_v(h = 0.99) = 17.4a$, well less than the system size chosen, and we avoid finite size effects. Other data are presented for $\lambda = 0.99$, for which $r_v(0) \approx 4.97a$, and $r_v(h = 0.99) = 35.2a$. In this latter case, some finite size effects might be expected in moderate sized systems as $h \rightarrow 1$.

In general, a given mode has a $e^{im\chi}$ spatial dependence on the azimuthal coordinate χ , where m is some integer. In fact, in the continuum theory [Sec. III B] m is a good quantum number, due to rotational invariance. This symmetry is weakly broken on a lattice, but for long-wavelength modes, m can be considered a good quantum number even on a lattice. At zero magnetic field, the modes $\pm m$ are degenerate when the anisotropy is strong enough to produce only stable in-plane vortices. For the weak easy-plane anisotropy considered here, the $\pm m$ modes on the stable out-of-plane (and cone state)

vortices are nondegenerate. All modes can also be labeled by a radial quantum number n , which is the number of nodes in the radial direction, including a node at the system boundary, due to our application of Dirichlet boundary conditions there.

In Figs. 6, 7 and 8 we show some of the lowest mode wavefunctions, with a single vortex present at the center of the system, and how these wavefunctions vary with the magnetic field. The system has $R = 20a$ and $\lambda = 0.99$. In these diagrams the $S^{\tilde{x}}$ (or $\varphi_{\mathbf{n}}$) amplitudes (certain magnitude and phase) are shown as arrows with triangular heads, and $S^{\tilde{y}}$ (or $\theta_{\mathbf{n}}$) amplitudes are shown as arrows with v-heads.³⁴ The number of rotations of the arrows as one moves along a contour around the vortex (at center of the system) is used to determine m . In most modes the $S^{\tilde{x}}$ (in-plane) fluctuations dominate, except when h approaches closer to 1.

In Fig. 9 we show the field dependence of some of the mode frequencies, calculated for $R = 30a$, where $h < 0$ corresponds to heavy vortices and $h > 0$ corresponds to light vortices. As h increases above 0, we see that the lowest ω_{+2} grows while the lowest ω_{-2} diminishes; the magnetic field induces a large splitting of this doublet compared to that at $h = 0$. For large enough negative h the splitting is reversed in sign. There are corresponding changes in the wavefunctions: the wavefunction for $m = +2$ becomes more spread out with increasing h , while the wavefunction for $m = -2$ becomes more centralized with increasing h . On the other hand, the lowest $m = -1$ mode becomes more spread out with increasing h , and more importantly, as $h \rightarrow h_c$ ($h_c \approx -0.6$), its wavefunction is very localized on the core of the vortex. Thus it appears that this mode could be associated with the instability of the heavy vortices at large negative h . Next we consider whether some of these features can be explained on theoretical grounds.

B. Theoretical analysis of magnon-vortex scattering

For the continuum description we consider small deviations ϑ, μ , from the static vortex solutions in the form

$$\varphi = q\chi + (\sin \theta_0)^{-1} \mu \quad , \quad \theta = \theta_0(r) + \vartheta. \quad (23)$$

The additional factor $(\sin \theta_0)^{-1}$ in (23) is introduced for convenience, making μ, ϑ , equivalent to the variables $S^{\tilde{x}}/S$ and $S^{\tilde{y}}/S$, respectively, introduced above for the analysis of modes in a lattice system.

Substituting (23) in the Landau-Lifshitz equations (6) and linearizing in ϑ and μ gives the following set of coupled partial differential equations, symmetric in ϑ and μ , with Schrödinger-type differential operators:

$$[-\nabla_x^2 + V_1(x)] \vartheta + \frac{2q \cos \theta_0}{x^2} \frac{\partial \mu}{\partial \chi} = -\frac{r_v}{c_0} \frac{\partial \mu}{\partial t}, \quad (24a)$$

$$[-\nabla_x^2 + V_2(x)] \mu - \frac{2q \cos \theta_0}{x^2} \frac{\partial \vartheta}{\partial \chi} = +\frac{r_v}{c_0} \frac{\partial \vartheta}{\partial t}. \quad (24b)$$

Here $x = r/r_v$ and $\nabla_x = r_v \nabla$, and the potentials $V_1(x), V_2(x)$ are

$$V_1(x) = \left(\frac{q^2}{x^2} - 1 \right) \cos 2\theta_0 + h \cos \theta_0, \quad (25a)$$

$$V_2(x) = \left(\frac{q^2}{x^2} - 1 \right) \cos^2 \theta_0 - \left(\frac{d\theta_0}{dx} \right)^2 + h \cos \theta_0. \quad (25b)$$

In order to solve (24) the following ansatz for ϑ and μ is appropriate:³⁰

$$\vartheta = \sum_n \sum_{m=-\infty}^{+\infty} f_\alpha(r) \cos(m\chi - \omega_\alpha t + \delta_m), \quad (26a)$$

$$\mu = \sum_n \sum_{m=-\infty}^{+\infty} g_\alpha(r) \sin(m\chi - \omega_\alpha t + \delta_m). \quad (26b)$$

$\alpha = (n, m)$ is a full set of numbers labeling the magnon eigenstates, with principle quantum number n and azimuthal quantum number m , and the δ_m are arbitrary phases. Substituting this ansatz gives an eigenvalue problem (EVP) having the form of coupled equations for the functions f, g ,

$$\left[\left(\frac{d^2}{dx^2} + \frac{1}{x} \frac{d}{dx} - \frac{m^2}{x^2} \right) - V_1(x) \right] f = \left(-\frac{\omega r_v}{c_0} + \frac{2qm \cos \theta_0}{x^2} \right) g \quad (27a)$$

$$\left[\left(\frac{d^2}{dx^2} + \frac{1}{x} \frac{d}{dx} - \frac{m^2}{x^2} \right) - V_2(x) \right] g = \left(-\frac{\omega r_v}{c_0} + \frac{2qm \cos \theta_0}{x^2} \right) f \quad (27b)$$

where the index α is omitted. Without loss of generality, at this point we choose the sign of the topological charge, $q = +1$. f and g cannot be determined analytically from Eqs. (27), but some useful results can be obtained without a full solution. Comparing Eqs. (26a) with the definition of the variables $S_{\mathbf{n}}^{\tilde{x}}, S_{\mathbf{n}}^{\tilde{y}}$ above, we see that the μ and ϑ fields are 90° out of phase, which implies that the $S^{\tilde{x}}$ and $S^{\tilde{y}}$ arrows in the wavefunction plots must be orthogonal. A related important result is that for pure modes with a well-defined value of m , a plot of the wavefunction corresponds to a vortex-like structure of the $S^{\tilde{x}}, S^{\tilde{y}}$ arrows with an apparent "vorticity" or winding number equal to m , as we saw above. This feature is useful for identification of m in the different modes obtained numerically for lattice systems.

The asymptotic behavior of f and g can be calculated also. For $r \rightarrow 0$ we obtain the same result as for $H = 0$, namely, $f, g \sim r^{|q+m|}$, which describes the presence of a 'hole' in the functions μ, ϑ , at the vortex core for large values of m . For large radius, in contrast with the case of zero field,³⁰ the asymptotics are more complicated, because the term with $\cos \theta_0$ in the RHS of equations

(27) does not fall exponentially, but only as h/x^2 . We show below that this produces a crucial difference in the magnon modes of these cases, namely, “giant doublet splitting”, which is a giant field dependence of the splitting, observed in the numerical calculations of the modes.

Consider the equations (27) far from the vortex. Using the asymptotics $\cos \theta_0 \approx h + h/x^2 + (h/x^4)(5 - h^2)/(1 - h^2)$, and keeping the terms with the lowest powers of the small function $1/x^2$ only, the potentials in these equations can be presented in the form

$$V_1 = 1 - h^2 - \frac{1 + h^2}{x^2}, \quad V_2 = \frac{h^2}{x^4}. \quad (28)$$

The potential V_1 having the term finite at $x \rightarrow \infty$, an expression for f in terms of g can be constructed as an expansion in powers of $1/x^2$. To do this, rewrite Eq. (27a) in lowest order in $1/x^2$,

$$\left[-\frac{d^2}{dx^2} - \frac{1}{x} \frac{d}{dx} + 1 - h^2 + \frac{m^2 - 1 - h^2}{x^2} \right] f = \left(\frac{\omega r_v}{c_0} - \frac{2mh}{x^2} \right) g. \quad (29)$$

Now let $g \propto Z_\nu(z)$, where Z is one of the cylindrical (Bessel) functions J_ν or Y_ν , and $z = kr$, where k is a magnon wave number whose value is determined by ω through the dispersion relation (7). The index ν will be allowed to differ slightly from the integer value m (we check this below). Then, in this lowest approximation f is also proportional to $Z_\nu(z)$, specifically, $f^{(0)} = \frac{\omega r_v}{c_0} (k^2 r_v^2 + 1 - h^2)^{-1} g$. Continuing this way, we can find f in the form, $f = f^{(0)}(1 + a/x^2 + b/x^4 + \dots)$. Also, assuming small k , with $kr_v \ll 1$, we arrive at

$$f = \frac{1}{1 - h^2 + k^2 r_v^2} \left(\frac{\omega r_v}{c_0} - \frac{2mh}{x^2} \right) g. \quad (30)$$

The expansion of f in the small quantities kr_v and $1/x^2$ could be constructed with arbitrary accuracy, but for our case it is enough to use this expression. Note that only the term with $2mh/x^2$ is kept here, because it can be as large as or larger than the first term when ω is small. Using this formula and Eq. (27b), far from the vortex we get an EVP for $g(z)$ only. It can be written as

$$\frac{d^2 g}{dz^2} + \frac{1}{z} \frac{dg}{dz} - \frac{\nu^2}{z^2} g + \frac{\kappa^2}{z^4} \cdot \frac{4h^2(1 + m^2)}{(1 - h^2)} g + g = 0, \quad (31)$$

where $\kappa = kr_v(0)$ and the index is given by

$$\nu^2 = m^2 + \frac{4mh\omega r_v(0)}{c_0(1 - h^2)}. \quad (32)$$

Thus, two unusual features are present for cone state vortices at nonzero magnetic field. First, non-integer ν appear, and second, terms like $1/x^4$ appear, caused by non-exponential decay of the out-of-plane spin components in the vortex. As was shown in Ref. (26), the

terms with $1/x^4$ are very important for the description of magnon scattering by Belavin - Polyakov solitons present in isotropic magnets. Accounting for these modifications changes not only coefficients but even the dependence of the scattering amplitude on k . To our knowledge, equations with non-integer ν have not appeared before in the description of soliton - magnon scattering. Next we discuss the role of these terms in detail.

Obviously, at large distances, $r \gg r_v$, the solution should describe the free magnons scattered by the vortex. For free magnons the solution is a combination of plane waves in a form $g^0 \propto \exp(i\vec{k} \cdot \vec{r})$, and $g_m = g_m^0 \propto J_m(kr)$. If a vortex is present we can use the scattering approximation, then the function g_m at $kr \rightarrow \infty$ could be rewritten as

$$g_m \propto J_m(kr) + \sigma_m Y_m(kr), \quad (33)$$

where $J_m(z), Y_m(z)$ are the Bessel and Neumann functions respectively, with *integer* index m , and the quantity $\sigma_m = \sigma_m(\kappa)$ (scattering amplitude) determines the intensity of the magnon scattering due to the presence of the vortex. If one writes $\sigma_m = -\tan \delta_m$, in standard notation for scattering problems, the S -matrix can be written as $S_m = \exp(2i\delta_m)$.

On the other hand, the solution of Eq. (31) without the terms κ^2/z^4 at $r \rightarrow \infty$ could be written as

$$g^{(0)} = J_\nu(z) + \tilde{\sigma}_m(\kappa) \cdot Y_\nu(z), \quad (34)$$

where the index of the Bessel and Neumann functions determined by Eq. (32) is *non-integer*. Then, at large but finite distances, some corrections caused by the term proportional to κ^2/z^4 in Eq. (31) must be taken into account. In the long-wave approximation, $\kappa \ll 1$, these corrections are small, and they decay faster than the cylindrical functions, but they are also important for the soliton-magnon scattering by the Belavin-Polyakov solitons in isotropic ferromagnets, as was shown in Ref (26). Therefore, for non-zero field, the solution can be written in the form

$$g_m = J_\nu(z) + \sigma_m(kr_v) \cdot Y_\nu(z) + \Delta g_m(k, z), \quad (35)$$

where the non-integer value $|\nu| \approx |m|$ is determined by Eq. (32), and $\Delta g_m(k, z)$ represents the contribution of the term with $(1/z^4)$ in Eq. (31).

The function $\Delta g_m(k, z)$ can be considered as a small correction, see Ref. 26 for details. The role of the term $\Delta g_m(k, z)$ could be important at small z , and this correction must be taken into account in the region $r_0 \ll r \ll 1/\kappa$, which is used for calculation of scattering amplitude $\sigma_m(\kappa)$ in the long wavelength approximation, see Refs. 30, 27, 26. For example, this term gives the dominant contribution to σ_m for all $|m + 1| > 1$, for Belavin-Polyakov solitons in isotropic ferromagnets.²⁶ But we have shown that for the cone state vortex case their accounting gives higher powers of small parameter kr_v to the scattering amplitude and these corrections could be

omitted. These terms are important for the analysis of magnon modes for the finite size magnet with $R \leq r_v$, see the last section. Thus, in contrast with the Belavin–Polyakov case, these corrections are unimportant in the scattering approximation (far from the vortex) and they can be omitted.

Now we are in a position to analyze the function g [Eq. (35)] describing magnon mode and magnon–vortex scattering. The most important thing for our problem is that the value of $\tilde{\sigma}_m(\kappa)$, see Eq. (34), could differ from the real scattering amplitude $\sigma_m(\kappa)$. In the long-wave approximation, this can be seen if we take into account that the terms with $\sigma_m(kr_v)$ and $r_v^2 k^2$, as well as the difference $|\nu - m|$, are small. Then, the Bessel function $J_\nu(z)$ can be expanded in powers of small quantity $|\nu - m|$ and represented through $J_m(z)$. Using the formula $(dJ_\nu/d\nu)_m \approx \pi Y_m/2$ at $z \rightarrow \infty$ see Ref. 35, and the concrete value of $\nu - m$ from Eq. (32), the desired relation between the $\tilde{\sigma}_m(\kappa)$ and the scattering amplitude $\sigma_m(\kappa)$ can be written as

$$\sigma_m(\kappa) = \tilde{\sigma}_m(\kappa) + \frac{\pi h \omega r_v}{c_0(1-h^2)} \text{sign } m. \quad (36)$$

The value of $\tilde{\sigma}_m(\kappa)$ is determined by the region near the vortex core,³⁰ and could be calculated using the same method as in this article. Note that for all the modes Eq. (36) predicts a linear dependence of $\sigma_m(\kappa)$ on the wave vector k . The same dependence occurs at $h = 0$ only for translational modes, with $m = \pm 1$. For the rest of the modes, with $m \neq \pm 1$, the scattering is smaller than that for the translational mode with $m = \pm 1$. As we show below, the same regularities are still valid for $\tilde{\sigma}_m(\kappa)$ at $h \neq 0$.

The value of $\tilde{\sigma}_m(\kappa)$ is determined by the region near the vortex core. At $h = 0$ it was calculated analytically, for $m = \pm 1$ in Ref. 30 and for $m = 0$ in Ref. 27. For other modes it was only investigated numerically. The important point is that the value of $\tilde{\sigma}_m(\kappa)$ for $m = \pm 1$ is largest at the long-wave limit (linear in k), the values of $\tilde{\sigma}_m(\kappa)$ are smaller for $m = \pm 2$ and $m = 0$ [the last one is proportional to $k^2 \ln(1/k)$,²⁷] and the scattering amplitudes for the other modes are negligibly small. Using this, we can omit the term $\tilde{\sigma}_m$ for all the modes with $m \neq 0, \pm 1$. The scattering amplitude of these modes, in the lowest approximation on $\omega r_v/c$, becomes

$$\sigma_m(k) = \frac{\pi h \omega r_v}{c_0(1-h^2)} \text{sign } m, \quad |m| > 1. \quad (37)$$

For the most interesting case, the translational modes with $|m| = 1$, the value of $\tilde{\sigma} \propto \kappa$, and we need to calculate it. It can be done in the same way as for $h = 0$, see Ref. 30; we discuss these calculations only briefly. We present $f(x)$, $g(x)$ in the form

$$f(x) = f^{(0)}(x)[1 + \alpha(x)], \quad g(x) = g^{(0)}(x)[1 + \beta(x)], \quad (38)$$

where $f^{(0)}(x)$, $g^{(0)}(x)$ are known zeroth solutions describing the soliton displacement,

$$f^{(0)}(x) = \frac{d\theta_0}{dx}, \quad g^{(0)}(x) = \text{sign}(m) \frac{\sin \theta_0}{x}, \quad (39)$$

and functions α , β are proportional to the small parameter $\omega r_v/c$. Then, in an approximation linear in α , β , and $\omega r_v/c$, for $x \gg 1$ one can get

$$(1-h^2)^{-1/2} g = \frac{r_0}{r} + \frac{m\omega r}{c_0|m|(1+h)} - \frac{2h\omega r_0^2}{rc_0(1+h)^2} \ln\left(\frac{r}{r_0}\right). \quad (40)$$

This equation at $h = 0$ coincides with one from Ref. 30. Comparing this expression with Eq. (33), in the region $1 \ll x \ll kr_0$, where both are valid, and using the asymptotics of the cylindrical functions for $z \ll 1$, specifically, $J_1 \approx z/2$, $Y_1 \approx -2/(\pi z)$, we arrive at the formula $\tilde{\sigma} = -(\pi\kappa^2 c_0 r_0/\omega)(1+h)\text{sign}(m)$. The logarithm in Eq. (40) gives higher powers of the small quantity κ , and the corresponding terms in $\tilde{\sigma}$ are omitted. Using Eq. (36), we can present the scattering amplitude $\sigma(\kappa)$ in the form

$$\sigma_{|m|=1} = -\frac{\pi\omega r_0}{4c_0} \text{sign}(m) \frac{1-3h}{1-h^2}. \quad (41)$$

For the mode with $m = 0$ the term linear in ω is absent, and the dependence $\sigma_0 \propto \omega^2 \ln \omega$ found for $h = 0$ ²⁷ still holds for $h \neq 0$. Thus, for all the modes with $|m| > 1$, the presence of the magnetic field changes the scattering amplitude drastically: terms linear in ω appear and the scattering amplitude at $h \neq 0$ becomes much larger than that for zero field. We find that this produces a large splitting of the doublets $\pm m$, which has been verified by our numerical calculations. More detailed investigation of these regularities, important for the description of magnon modes for small particles in the so-called vortex state,²¹ will be carried out in the next section.

IV. MAGNON MODES FOR CIRCULAR MAGNETIC PARTICLE IN THE VORTEX CONE STATE

As was shown in Ref. 30, the scattering amplitude is a very convenient tool for calculation of frequencies of magnon modes for finite sized circular magnets. This amplitude can be calculated analytically, or numerically with the use of a shooting method^{30,28,26,27} for infinite system size, or extracted from numerical diagonalization for discrete finite size systems with particular boundary conditions. If the function $\sigma_m(\kappa)$ is known, it is easy to calculate magnon frequencies for *arbitrary* system sizes and boundary conditions. For example, in Ref. 30 the values of $\sigma_m(\kappa)$ taken from numerical data for the magnet with fixed (Dirichlet) b.c. and sizes $R = 20a$ to $R = 100a$ were brought together and used to describe

the computer simulation of the vortex oscillations for the $R = 72a$ system with free b.c.

During recent years the problem of magnon modes for finite size magnetic particles has become very important in connection with novel magnetic materials – granular magnets or magnetic dot arrays. These magnetic dots are micron sized islands on a non-magnetic substrate, made from different soft magnetic materials and having different shapes – circular, elliptical or rectangular. They are interesting both from the practical (high-density magnetic storage media) and fundamental points of view, see Refs. 20. Resonance experiments for such dot arrays show the presence of discrete magnon modes³⁶ caused by space quantization due to the finite dot size.

The theory of such modes was constructed for *homogeneous* in-plane magnetization.³⁷ On the other hand, it is known that small particles can be in different inhomogeneous states, namely, vortex states,²¹ and so-called leaf or flower states.³⁸ In this section, we apply our vortex-magnon scattering theory to a finite-sized circular magnet in the cone vortex state. Note that we do not intend a quantitative description of the magnon modes in a real circular or cylindrical particle in the vortex state. The vortex state is formed by the long-range magnetic dipole interaction,²¹ and this interaction is not included in our model, but does play an important role in forming the magnon mode spectrum, see Ref. 37. On the other hand, the main features of the model investigated below, such as the doublet splitting and the presence of anomalous low frequencies, must be model-independent and present for real particles in vortex states.

We discuss the magnon modes for a two-dimensional circular magnet with radius R (or, a thin cylinder) and some boundary condition at $r = R$. For definiteness, we apply fixed boundary conditions, $\theta = \theta_0$ at $r = R$. For $h = 0$ and large enough $R \gg r_v$, the frequencies are completely determined by the scattering amplitude,³⁰ but for the cone state the situation is more complicated.

As was shown in the previous section, due to the slow (power) decay of the out-of-plane magnetization in the vortex, the correction $\Delta g_m(k, z)$ proportional to $k^2 h^2$ appears in the solution [See Eq. (35)]. Moreover, the equation $(dJ_\nu/d\nu)_{\nu=m} = (\pi/2)Y_m$, used for the derivation of the scattering approximation, is only valid at argument $kr \gg 1$.

But for the more interesting low-frequency magnon modes, with small principal quantum numbers n , the values of kR are not large; in the lowest approximation the boundary conditions force kR to be zeros of Bessel functions, see below. Thus, the universal connection between $\sigma(\kappa)$ and magnon frequencies at $h \neq 0$ can be established only for $n \gg 1$. To investigate the cases of interest, $n = 1, 2, \dots$, one needs to use the exact formula for $(dJ_\nu/d\nu)_{\nu=m}$ and take into account the corrections caused by the terms $1/z^4$ in Eq. (31).

This is a complicated problem, the full solution of which is far from the aim of this article. Two interesting limiting cases are considered here. The first is the case

of small field, where the correction $\Delta g_m(k, z)$, quadratic in h , can be omitted. For small fields the vortex core size is equal to r_0 , and it could be much less than the system size R . The second case deals with the limit $H \approx H_a$. There the vortex core size W grows as $H \rightarrow H_a$, and for arbitrarily large values of R/a , the values of W and R become comparable for some H nearly equal to H_a . Obviously, the scattering approximation fails in this limit, and to describe it a special technique is presented below.

A. Large system size, small field

To calculate the magnon modes for small but nonzero field, the correction $\Delta g_m(k, z)$ can be omitted, and it is more convenient to present the solution (33) through J_ν and $J_{-\nu}$ instead of J_m and Y_m ,

$$g_m = J_\nu(z) + \tilde{\sigma}_\nu(\kappa)J_{-\nu}(z), \quad (42)$$

where ν is considered a *positive* non-integral number, $\nu = |m| + (2h\omega r_0/c)\text{sign}(m)$, for $h \ll 1$, $h \neq 0$. The function $\tilde{\sigma}_\nu(\kappa)$ can easily be written through $\tilde{\sigma}_m(\kappa)$; it is zero in the absence of scattering.

For modes with $m \neq 0, \pm 1$, the values of $\tilde{\sigma}$ (or $\tilde{\sigma}$) are negligibly small, and the b.c. immediately gives us the equation for the frequencies of the modes with given m, n , in the form $\omega_{m,n} = j_{\nu,n}c(h)/R$, where $j_{\nu,n}$ is the n^{th} zero of $J_\nu(z)$. Thus, for small $\nu - |m|$, and $c(h) \approx c_0$, the frequency for $m \neq 0, \pm 1$ takes the form,

$$\omega_{m,n} = \omega_{m,n}^{(0)} + \delta\omega_{m,n}, \quad (43)$$

where $\omega_{m,n}^{(0)}$ determines the frequency in the main approximation on a/R , and depends on $|m|$,

$$\omega_{m,n}^{(0)} = \frac{c_0 j_{m,n}}{R}. \quad (44)$$

As for the homogeneous case, it is seen that in this approximation, doubly degenerate modes (i.e., doublets) appear. The next correction $\delta\omega_{m,n}$ can be written as

$$\delta\omega_{m,n} = 2hJS \left(\frac{a}{R}\right)^2 \text{sign}(m)j_{m,n} \left(\frac{dj_{\nu,n}}{d\nu}\right)_{\nu=m}. \quad (45)$$

This term produces the characteristic feature of magnon modes for vortex state particles, namely, the splitting of the doublets. This splitting is clearly seen in numerical results, see Fig. 9. This splitting for $m \neq 0, \pm 1$ is proportional to the magnetic field,

$$\begin{aligned} \Delta\omega_{|m|,n} &\equiv \omega_{|m|,n} - \omega_{-|m|,n} \\ &= 4hJS \left(\frac{a}{R}\right)^2 j_{m,n} \left(\frac{dj_{\nu,n}}{d\nu}\right)_{\nu=|m|}. \end{aligned} \quad (46)$$

The values of $(dj_\nu/d\nu)_{\nu=|m|}$ can be expressed through some long, but finite combinations of Bessel functions, see

Ref. 35, or found numerically. At $n \gg 1$, the simple expression $(dj_\nu/d\nu)_{\nu=|m|} = (\pi/2)[N_m(j_{m,n})/J'_m(j_{m,n})]$ can be used.

The formula (46) is in good agreement with our numerics for $m = 2, 3, 4$ (only $n = 1$ was considered). For comparison of the analytical and numerical results the dimensionless quantity

$$\begin{aligned} \Delta\Omega &\equiv \Delta\omega \cdot (R/a)^2(1/JS) \\ &= 4h[j_{\nu,n} \cdot (dj_{\nu,n}/d\nu)]_{\nu=m}, \end{aligned} \quad (47)$$

is most convenient. Some doublet splitting results from numerical simulations for $|m| > 1$ on an $R = 30a$ system are shown in Fig. 10. For $n = 1$ the theory gives $\Delta\Omega_{m=2}/h = 26.09$ [with $(dj_\nu/d\nu)_2 = 1.27$], while the slope of the $\Omega_{m=2}(h)$ data is approximately 29.2; theory gives $\Delta\Omega_{m=3}/h = 31.39$ [with $(dj_\nu/d\nu)_3 = 1.23$], whereas the slope from numerical results for $\Omega_{m=3}(h)$ is approximately 34.5; theory for $m=4$ gives $\Delta\Omega_{m=4}/h = 36.4$, while the slope from the data is 39.1. Similar calculations of these slopes by numerical simulation on an $R = 25a$ system gave values of 32.6, 35.2, and 39.1, for $m = 2, 3, 4$, respectively. Note that the numerical data do not go exactly through $\Delta\Omega = 0$ at $h = 0$, due to the breaking of the degeneracy there caused by the lattice. However, the trends of slopes increasing with m are consistent with the theory, and the linear dependence on h is verified, provided h is not too close to $+1$.

For modes with $m = \pm 1$ it is necessary to calculate the value of $\tilde{\sigma}_m$. For the lowest (the translational Goldstone mode, TGM), it is enough to use the expansion (40), which gives

$$\omega_{-1,1} \equiv \omega_{TGM} = JS(1+h) \left(\frac{a}{R}\right)^2. \quad (48)$$

The appearance of a mode with extremely low frequency, $\omega_{TGM} \ll \omega_{m,n}^{(0)} \propto (a/R)$, is a specific feature of large enough systems in the vortex state. The theoretical prediction, Eq. (48), agrees very well with the numerical simulations for h near zero, see Fig. 11.

For other modes with $|m| = 1$, the splitting of the doublets is

$$\begin{aligned} \Delta\omega_{m,n} &= -2JS \left(\frac{a}{R}\right)^2 j_{1,n} \times \\ &\left\{ \frac{\pi}{2}(1+h) \frac{N_1(j_{1,n})}{J'_1(j_{1,n})} - 2h \left(\frac{dj_{\nu,n}}{d\nu}\right)_{\nu=1} \right\}. \end{aligned} \quad (49)$$

For $h = 0$, this coincides with results in Ref. 30. For these modes, $\omega(m = -1)$ in the same doublet is higher than $\omega(m = 1)$. For $n = 1$, and using $(dj_{\nu,1}/d\nu)_{\nu=1} \approx 1.34$, the splitting of the lowest doublet can be written

$$\Delta\omega_{1,1} = JS \left(\frac{a}{R}\right)^2 (6.157 - 14.38h), \quad (50)$$

a result that is found to be in reasonable agreement with our numerical data, as shown in Fig. 11.

B. Small system size and large field

In the previous subsection we have shown for the finite system that as the field increases the translational mode frequency grows, $\omega_{TGM} \propto (1+h)/R^2$, but the other mode frequencies decrease, $\omega_{m,n} \propto \sqrt{1-h^2}/r_v R$. It is clear that the frequencies of these modes become comparable at some value of the magnetic field. Comparing the formulas for ω_{TGM} and $\omega_{m,n}$ one can see that they are comparable when $(1-h) \sim (1+h)(r_v/R)^2$, i.e. when $R \sim r_v/\sqrt{1-h^2} \simeq r_v(h)$. Thus, it happens at fields such that the vortex core size $r_v(h)$ becomes comparable with the system size R . It is seen that frequency of the lowest mode with $m = -1$ (the mode of vortex translational motion) has the same order of magnitude as other modes.

This limiting case, $R \ll r_v(h)$, is unrelated to the vortex dynamic problem in the infinite FM. However, it precisely appears to be most fascinating for another actual problem, namely, the problem of the eigenmodes for small ferromagnetic particles in a non-uniform vortex state. Therefore, let us go into details.

In the limiting case $R \ll r_v(h)$, one can expect that characteristic gradient values of $\theta_0(r)$ are considerably higher than that for a vortex in an infinite FM at the same field. Then, within the main approximation in a small parameter $R/r_v(h)$, Eq. (10) only has terms containing derivatives $\theta_0(r)$ or the term with $1/r^2$. This means that anisotropy and magnetic field energies can be disregarded here, i.e. the case of the isotropic model is in fact realized. For the isotropic FM, in this approximation Eq. (10) might be integrated once, which gives $d\theta_0/dr = (1/r) \sin \theta_0$. Then the analysis is simplified, and the soliton structure can be found exactly³⁹. Taking into account the boundary conditions, $\theta_0(0) = 0$, $\theta_0(R) = \theta_\infty$, the soliton structure is determined by the formula $\tan(\theta/2) = (r/R) \tan(\theta_\infty/2)$. The calculation of the small corrections caused by the anisotropy energy and the magnetic field gives the solution in the form of a series expansion in powers of small parameters $r/r_v(h) \leq R/r_v(h)$,

$$\begin{aligned} \tan\left(\frac{\theta}{2}\right) &= \left(\frac{r}{R}\right) \tan\left(\frac{\theta_\infty}{2}\right) \times \\ &\frac{1 + (r^3/24r_v^2R)(1-h) [(r^2/R^2) - 3]}{1 - R^2(1-h)/12r_v^2} \end{aligned} \quad (51)$$

An analysis of the normal modes on the background of this soliton in the isotropic case is also considerably simpler than for the anisotropic magnets. In particular, one can exactly construct the normal mode wave functions at $\omega \rightarrow 0$ ²⁵ and reveal their structure for small ω .²⁶ On the basis of these solutions one can solve the problem even for non-small θ_∞ , that corresponds to $1-h \sim h$ and $R \sim r_v$.

But we are only interested in the case $R \ll r_v(h)$, that requires $1-h \ll 1$. Then the further analysis will be carried out for this limiting case. Therewith we restrict

ourselves to a linear approximation in $1-h$. In this case it is convenient to write the Eqs. (24) as the set of equations for the functions $u = (f+g)/2$ and $v = (f-g)/2$, which at $\theta \ll 1$ are easily presented in the form

$$-\frac{d^2u}{dx^2} - \frac{1}{x} \frac{du}{dx} + \frac{(m+1)^2}{x^2}u + U(x)u + \frac{1}{2}V(x)v = \frac{\omega r_v}{c_0}u, \quad (52a)$$

$$-\frac{d^2v}{dx^2} - \frac{1}{x} \frac{dv}{dx} + \frac{(m-1)^2}{x^2}v + U(x)v + \frac{1}{2}V(x)u = -\frac{\omega r_v}{c_0}v, \quad (52b)$$

where both $U(x)$, $V(x)$ are small (linear in $1-h$) at $h \rightarrow 1$,

$$U(x) = \left(2 - \frac{h}{2} - \frac{m+2}{x^2}\right)\theta_0^2 - (1-h) - \frac{1}{2}V(x) \quad (53a)$$

$$V(x) = \left(\frac{d\theta_0}{dx}\right)^2 + \left(1 - \frac{1}{x^2}\right)\theta_0^2 \quad (53b)$$

In the limit of $h \rightarrow 1$ this system transforms to two uncoupled equations, which go over into each other by substituting m for $-m$ and ω for $-\omega$. It is clear that for the solutions with $\omega > 0$ we are interested in, for small $(1-h)$, the function $v \sim (1-h)u \ll u$. Then, the contribution of the term with v is of the order $(1-h)^2$ and it can be omitted. Consequently, the eigenmodes of the system are determined by a causal Schrödinger EVP for $u(x)$ derived from (52a). In a zeroth approximation its solution can be written in terms of Bessel function $J_\nu(kr)$ with integer index $\nu^2 = (m+1)^2$. Using the boundary conditions $u(R) = 0$ one obtains a zeroth solution,

$$u(r) = J_\nu(j_{\nu,n}r/R), \quad \omega_{m,n} = JS(a j_{|m+1|,n}/R)^2. \quad (54)$$

where $\nu = |m+1|$ and $j_{\nu,n}$ is the n -th zero of the Bessel function $J_\nu(x)$. It is easy to see that within the zeroth approximation in $(1-h)$ (i.e., $h = 1$), the modes with $m = -1 + \nu$ and $m = -1 - \nu$, where ν is a positive integer, have the same frequencies and at $m \neq -1$ form doublets. For small enough values of $(1-h)$, we have a linear vortex profile (as in Fig. 1): $\theta(r) \approx (r/R)\theta_\infty$, with $\theta_\infty^2 \approx 2(1-h)$. Then the potential $U(x)$ is proportional to $(1-h)$:

$$U(x) \approx - \left\{1 + 2 \left(\frac{r_v}{R}\right)^2 [(m+2) - x^2]\right\} (1-h). \quad (55)$$

Calculating the contribution of the potential $U(x)$ within perturbation theory, the eigenfrequencies can be presented as

$$\omega_{m,n} = JS \left(\frac{a}{R}\right)^2 \left\{ j_{|m+1|,n}^2 - \left[2(m+2) + \frac{R^2}{3r_v^2} \left(1 - \frac{4(\nu^2-1)}{j_{|m+1|,n}^2}\right)\right] (1-h) \right\}. \quad (56)$$

Thus, this degeneracy disappears if one takes into account the terms linear in $(1-h)$. Both the presence of the doublets containing the modes with $m = -1 \pm \nu$ and the splitting of these doublets linear in $(1-h)$ are in good agreement with the numerical data at $h \approx 1$. For modes which do not manifest discreteness effects and have well-defined m , Eq. (56) gives a fairly good quantitative agreement with the numerical data. These data can be fit by the function $\omega_{m,n}R^2/JS^2a^2 = A_{m,n}^{(0)} + A_{m,n}(1-h)$ with good accuracy, comparing results of numerical simulations for $R = 30a$ with the theoretical expression (56), see Table I. The values of $A_{m,n}^{(0)}$ are consistently within a few percent of the theoretical value, $j_{|m+1|,n}^2$. The coefficient $A_{m,n}$ does not depend on n for $\nu = |m+1| = 1$ and it can be presented as $-2(m+2) - 12.1$, which describes well the observed values of $A_{0,1}$, $A_{0,2}$, and $A_{-2,1}$, $A_{-2,2}$. Generally, the trends of the $A_{m,n}$ coefficients as m, n increase are correctly predicted, such as the reversals of sign seen for $m = -4, -5$, although the actual numerical values are less accurately described. Also, the formula (56) shows that the splitting $\Delta\omega_\nu = \omega_{-1-\nu} - \omega_{-1+\nu}$ of the doublets can be written, for fixed n , as $\Delta\omega_\nu R^2/JS^2a^2 = 4\nu(1-h)$. So the slope of the splitting vs. $(1-h)$ is predicted to be 4ν , independent of n ; the data of Table I give slopes of 3.6, 9.1, and 12.4 for $n = 1$ and $\nu = 1, 2, 3$, respectively, and a slope of 4.3 for $n = 2, \nu = 1$, consistent with the theory.

For those doublets in which the mix of the states with various m (for instance $m = 1$ and -3) occurs due to discreteness effects, the limiting value of the frequency at $h = 1$ is reasonably well described by the expression. The term depending on $(1-h)$ in (56), however, deduced under the assumption of an individual m in the mode, does not describe the observed h -field dependencies for these partially superposed modes. For example, for modes with $m = 1$ and $m = -3$ ($\nu = 2$), there are notable differences between the simulation and theory results for the $A_{m,n}$ coefficients (Table I); see also the $\nu = 4$ doublet. However, for the field dependence of the mean doublet frequency, $(\omega_{-1-\nu,n} + \omega_{-1+\nu,n})/2$, the simulation and theory results have somewhat better agreement. However, the doublets at $\nu = 2, \nu = 4$ are split even at $h = 1$, due to discreteness effects of the lattice, and it is clear that this makes application of Eq. (56), derived from continuum theory, problematical for these cases. With this exception, however, the theory given here enables us to describe eigenfrequencies with a given m in the case $r_v \ll R \ll r_v(h)$.

V. CONCLUSIONS

Easy-plane anisotropy combined with a magnetic field perpendicular to the easy plane leads to interesting new features in the vortex properties and their effect on the scattering of magnons. This combination of anisotropy and field leads to the so-called cone state, where the

spins tilt at an angle determined by the magnetic field relative to anisotropy strength, $\cos\theta_0 = h$, at an arbitrary in-plane angle. In the presence of weak anisotropy [$(1 - \lambda) < 0.28$ for square lattice], the stable out-of-plane vortices are modified by the magnetic field into light and heavy branches, depending on whether the magnetic field is aligned with ($h > 0$) or contrary to ($h < 0$) the out-of-plane component (S^z) of the vortex. In the limit $h \rightarrow 1$, the light vortex energy goes to zero, as seen in Fig. 4, and the vortex width becomes larger than the system size. On the other hand, at large negative magnetic field, the heavy vortex width decreases, and at a certain critical field $h_c < 0$, the vortex becomes unstable. Beyond this limit there are no heavy vortices; the central core region spins reverse and the vortex transforms to a light vortex. This instability can be explained as due to discreteness effects of the lattice, which can be accounted for, to leading order, by including fourth order derivative terms in the continuum limit Hamiltonian, together with a variational ansatz for the vortex out-of-plane structure. This theory also gave a reasonable description of the dependence of h_c on the easy-plane anisotropy strength $(1 - \lambda)$, as presented in Fig. 5.

The presence of a cone state vortex modifies the spectrum of magnons, which we analyzed through a numerical relaxation procedure and through analysis of the dynamical oscillations about the vortex structure. The most significant effect of the magnetic field on this spectrum is its influence on doubly degenerate modes. For small fields $|h| \ll 1$, pairs of modes $\omega_{\pm m, n}$, with $|m| > 1$, that are nearly degenerate at $h = 0$, obtain a splitting proportional to the magnetic field. The frequency of the mode with $m > 0$ increases with h , while the frequency of the mode with $m < 0$ decreases with h . Lack of exact degeneracy at $h = 0$ is attributed to the scattering amplitude $\tilde{\sigma}_m(\kappa)$ [See Eq. (34)], which is small but nonzero even at $h = 0$, as well as to lattice effects. For the modes with $|m| = 1$, there is also a linear dependence of the frequency on h at small fields, although a finite splitting is present in these doublets even at $h = 0$.

In the limit $h \rightarrow 1$, a different set of doublets is present, those with equal values of $|m + 1|$, or equivalently, the pairs with $m = -1 \pm \nu$, where ν is a positive integer. This clearly appears in Fig. 9. For these doublets, the mode with the more negative m is higher in frequency, and their splitting is proportional to $(1 - h)$, with the pairs being very close to degenerate at $h = 1$ (except for small effects due to the lattice).

This latter limit also is relevant for consideration of modes in small magnetic particles: when the particle size is smaller than the vortex core size for that magnetic field [$R \ll r_v(h)$], this leads to the presence of the weakly split doublets near $h \rightarrow 1$. Also, such particles will be expected to have an anomalously low frequency mode (the translational Goldstone mode) once the magnetic field is adjusted to small values $h \ll 1$. The general features found in the model system considered here are expected to appear in real particles, although the details

due to influence of different geometry and dimensionality may be different. Thus it may be interesting to look for either type of weakly split doublets, either near $h = 0$ or near $h = 1$, in resonance experiments on small particles supporting vortex states.

Acknowledgements— This work was partially supported by NSF DMR-9412300. One of the authors (B.I.) thanks Kansas State University for a kind hospitality and Grant INTAS-97 31311 for partial support.

-
- ¹ R. J. Donnelly, *Quantized Vortices in Helium II*, Cambridge Studies In Low Temperature Physics Vol. 3, Edited by A. M. Goldman, P. V. E. McClintoc, and M. Springford, (Cambridge University Press, Cambridge, 1991).
 - ² P. C. DeGennus, *Superconductivity of Metals and Alloys* (W. A. Benjamin, Inc., New York, Amsterdam, 1966).
 - ³ G. Blatter, M. V. Feigelman, V. B. Geshkenbein, A. I. Larkin, and V. M. Vinokur, *Rev. Mod. Phys.* **66**, 1125 (1994).
 - ⁴ M. R. Mathews, B. P. Anderson, P. C. Halljan et al, *Phys. Rev. Lett.* **83**, 2498, (1999).
 - ⁵ K. W. Madison, F. Chevy, W. Wohlleben, and J. Dalibard, *Phys. Rev. Lett.* **84**, 806, (2000).
 - ⁶ A. M. Kosevich, B. A. Ivanov, and A. S. Kovalev, *Phys. Rep.* **194**, 117 (1990).
 - ⁷ V. G. Bar'yakhtar and B. A. Ivanov, in *Soviet Scientific Reviews, Section A. Physics*, I. M. Khalatnikov (ed.), Vol. 16, No. 3 (1993).
 - ⁸ B. A. Ivanov and A. K. Kolezhuk, *Low Temp. Phys.* **21**, 275 (1995)
 - ⁹ V. L. Berezinskii, *Sov. Phys. JETP* **32**, 493 (1970); **34**, 610 (1972).
 - ¹⁰ J. M. Kosterlitz and D. J. Thouless, *J. Phys. C6* , 1181 (1973).
 - ¹¹ J. M. Kosterlitz, *J. Phys. C7*, 1046, (1974).
 - ¹² D. L. Huber, *Phys. Rev. B26*, 3758 (1982).
 - ¹³ F. G. Mertens, A. R. Bishop, G. M. Wysin and C. Kawabata, *Phys. Rev. Lett.* **59**, 117 (1987); *Phys. Rev. B* **39**, 591 (1987).
 - ¹⁴ D.D. Wiesler, H. Zabel and S.M. Shapiro, *Z.Phys.B: Condensed Matter* **93**, 277 (1994).
 - ¹⁵ B. A. Ivanov and D.D. Sheka, *Low Temp. Phys.* **21**, 881 (1995).
 - ¹⁶ L.P. Pitaevskii, *Sov. Phys.-JETP*, **13**, 451 (1961); E.P. Gross, *Nuovo Chimento* **20**, 454 (1961)
 - ¹⁷ J. Cristou, V. Tikhonenko, Yu.S. Kivshar, and B. Luther-Davids, *Opt. Lett.* **21**, 1649 (1996).
 - ¹⁸ A. A. Thiele, *Phys. Rev.* **30**, 230 (1973); *J. App. Phys.* **45**, 377 (1974).
 - ¹⁹ B. A. Ivanov and D.D. Sheka, *Phys. Rev. Lett.* **72**, 404 (1994).
 - ²⁰ J.F. Smyth, S. Schultz, D.R. Fredkin, D.P. Kern, S.A. Rishton, H. Schmid, M. Cali, and T.R. Koehler, *J. Appl. Phys.* **69**, 5262 (1991) ; A. Maeda, M. Kume, T. Ogura,

K. Kukkori, T. Yamada, M. Nishikawa, and Y. Harada, J. Appl. Phys. **76**, 6667 (1994); B. Hillebrands, C. Mathieu, C. Hartmann et al, J. Magn. Magn. Mat. **175**, 10 (1997).

²¹ N.A. Usov and S.E. Peschany, J. Magn. Magn. Mater. **118**, L290 (1993).

²² K. Runge, T. Nozaki, U. Okami et. al., J. Appl. Phys. **79**, 5075 (1996); R.P. Cowburn, D.K. Koltsov, A. O. Adeyeye et al., Phys. Rev. Lett. **83**, 1042 (1999); A. Fernandez and C.J. Cerjan, J. Appl. Phys. **87**, 1395 (2000); Jing Shi, S. Tehrani and M. R. Scheinfein, Appl. Phys. Lett., **76**, 2588 (2000); T. Pokhil, D. Song and J. Nowak, J. Appl. Phys. **87**, 6319 (2000).

²³ G. M. Wysin, Phys. Rev. B **49**, 8780 (1994).

²⁴ G. M. Wysin and A. R. Volkel, Phys. Rev. B **52**, 7412 (1995); **54**, 12,921 (1996).

²⁵ B. A. Ivanov, JETP Lett. **61**, 917 (1995).

²⁶ B. A. Ivanov, V. M. Murav'ev, and D. D. Sheka, JETP **89**, 583 (1999).

²⁷ B. A. Ivanov and I. A. Yastremsky, Low Temp. Phys. **26**, No. 5, 466, (2000).

²⁸ B. A. Ivanov, A. K. Kolezhuk, and G. M. Wysin, Phys. Rev. Lett. **76**, 511 (1996).

²⁹ D.D. Sheka, B.A. Ivanov, and F.G. Mertens, Phys. Rev. B **58**, 024432 (2001).

³⁰ B. A. Ivanov, H. J. Schnitzer, F. G. Mertens and G. M. Wysin, Phys. Rev. B **58**, 8464 (1998).

³¹ E.G. Galkina and B. A. Ivanov, JETP Lett **61**, 511, (1995).

³² N. Cooper. Phys. Rev. Lett. **80**, 4554 (1998); N. Papanikolaou and P. N. Spathis, Nonlinearity **12**, 285 (1999); A. A. Zhmudskii and B. A. Ivanov, JETP **86**, 1511 (1998).

³³ G. M. Wysin, Phys. Rev. B **63**, 94,402 (2001).

³⁴ See Ref.²⁴ for a more precise definition of the spin fluctuation amplitudes presented in our wavefunction plots.

³⁵ M. Abramowitz and I. A. Stegun, *Handbook of Mathematical Functions*, National Bureau of Standards Applied Mathematics Series, Vol. 55 (1964).

³⁶ C. Mathieu, J. Jorzick, A. Frank et. al, Phys. Rev. Lett. **81**, 3968 (1988).

³⁷ K. Yu. Guslienko, A. N. Slavin, J. Appl. Phys. **87**, 6337 (2000).

³⁸ M. Grimsditch, Y. Jaccard, and I. K. Shuller, Phys. Rev. B **58**, 11,539 (1998); N. A. Usov and S. E. Peschany, J. Magn. Magn. Mater. **130**, 275 (1994); R. P. Cowburn and M. E. Welland, Phys. Rev. B **58**, 9217 (1998); R. P. Cowburn, A. O. Adeyeye, and M. E. Welland, Phys. Rev. Lett. **81**, 5415 (1998).

³⁹ A. A. Belavin and A. M. Polyakov, JETP Lett. **22**, 245 (1975).

2	-3,1	25.664 / 26.375	-1.42 / -4.61
0	-1,2	29.671 / 30.471	-14.3 / -15.7
3	2,1	39.608 / 40.706	-8.93 / -10.6
3	-4,1	39.608 / 40.706	+3.50 / +1.41
1	0,2	47.863 / 49.219	-14.9 / -16.1
1	-2,2	47.863 / 49.219	-10.6 / -12.1
4	3,1	55.768 / 57.583	-3.15 / -9.49
4	-5,1	56.159 / 57.583	+3.67 / +6.51

TABLE I. Magnetic field dependence near $h \rightarrow 1$ for modes of an FM system with radius $R = 30a$ and $\lambda = 0.99$. The mode frequencies were fit to the form $\omega_{m,n}R^2/(JSa^2) = A_{m,n}^{(0)} + A_{m,n}(1-h)$, with simulation and theory results [Eq. (56)] compared.

ν	m,n	$A_{m,n}^{(0)}$ (sim./th.)	$A_{m,n}$ (sim./th.)
0	-1,1	5.6412 / 5.7832	-21.1 / -22.5
1	0,1	14.312 / 14.682	-14.5 / -16.1
1	-2,1	14.312 / 14.682	-10.9 / -12.1
2	1,1	25.677 / 26.375	-10.5 / -12.6

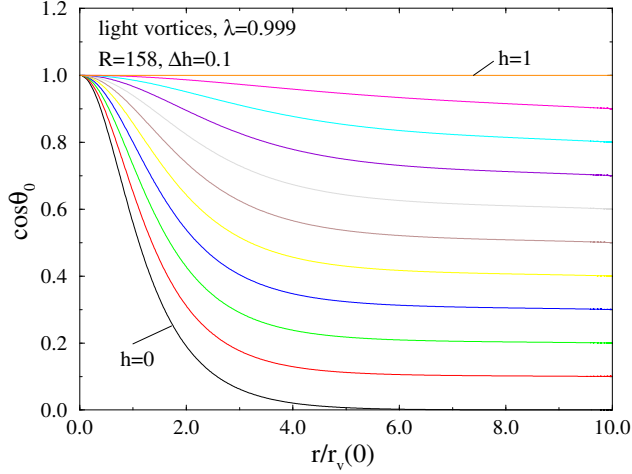


FIG. 1. The OP-vortex profiles for light vortices ($h > 0$) calculated using $\lambda = 0.999$ on a lattice system with radius $R = 158a$. The different curves correspond to different values of h with increment $\Delta h = 0.1$.

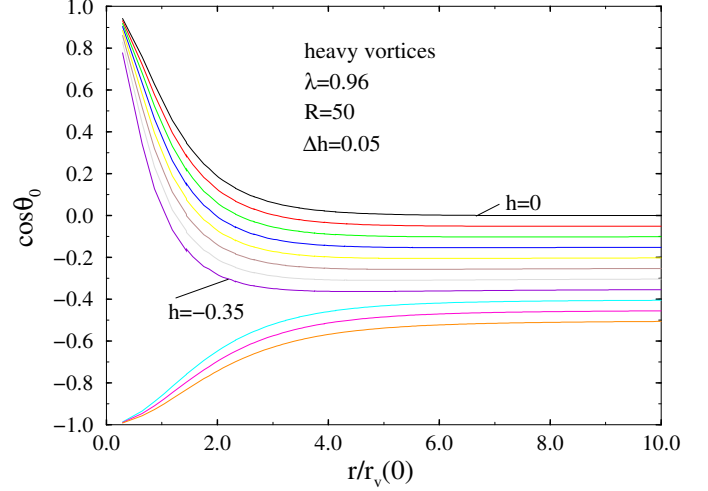


FIG. 3. The OP-vortex profiles for heavy vortices ($h < 0$) calculated using $\lambda = 0.96$ on a lattice system with radius $R = 50a$. The different curves correspond to different values of h with increment $\Delta h = -0.05$. There are no stable heavy vortices for h stronger than approximately 0.35; instead they converted to light vortices by reversal of spins in the core.

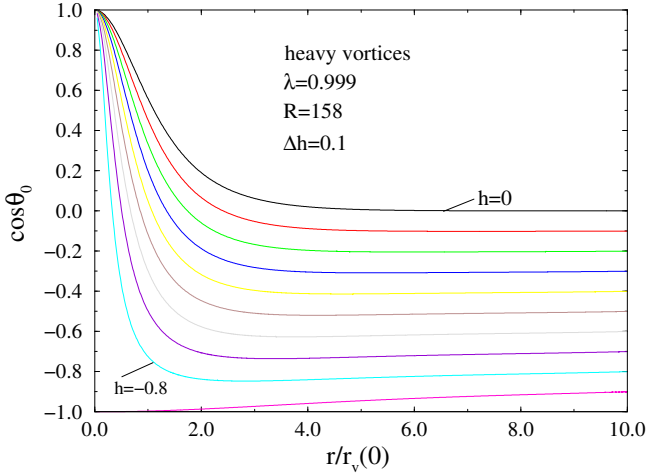


FIG. 2. The OP-vortex profiles for heavy vortices ($h < 0$) calculated using $\lambda = 0.999$ on a lattice system with radius $R = 158a$. The different curves correspond to different values of h with increment $\Delta h = -0.1$.

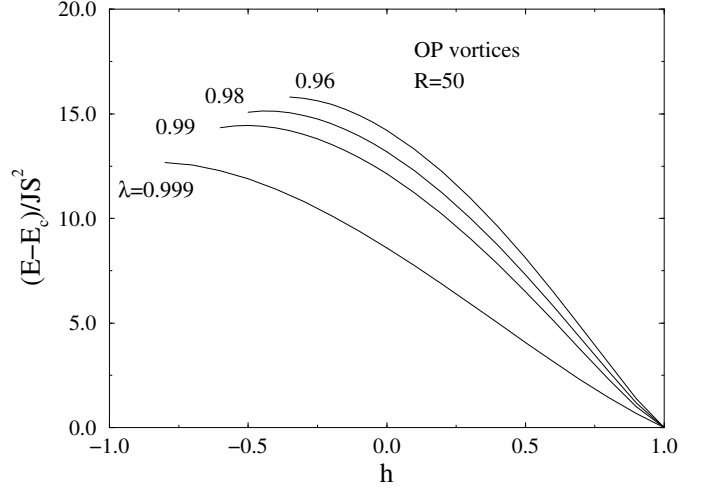


FIG. 4. The OP-vortex energies with the ground state energy of the cone state, E_c , subtracted out, for various values of the anisotropy parameter, λ . For $h > 0$ these are light vortices, and for $h < 0$ they are the heavy vortices. All were calculated on a lattice system with radius $R = 50a$.

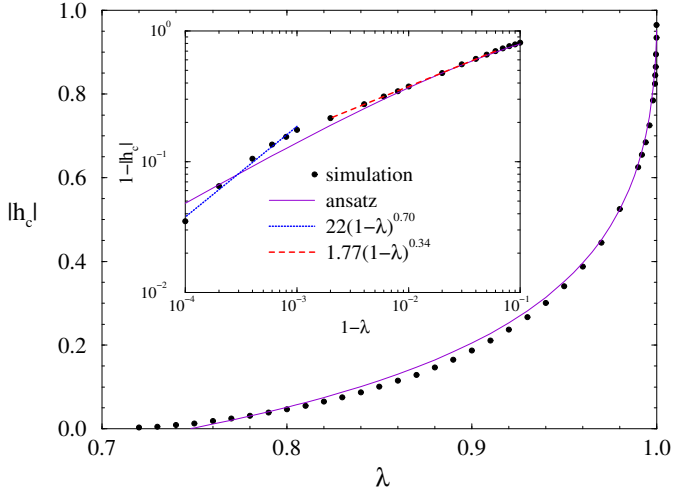
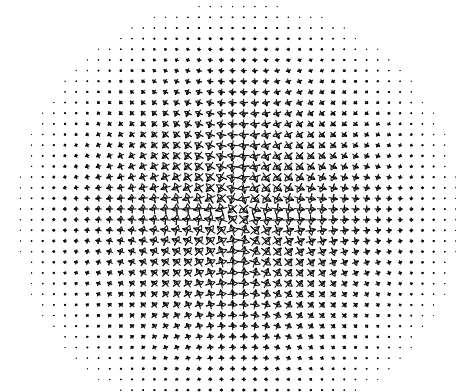
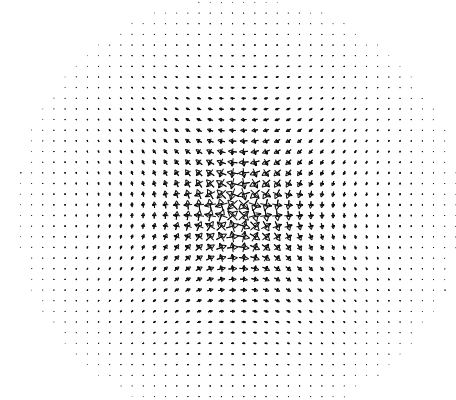


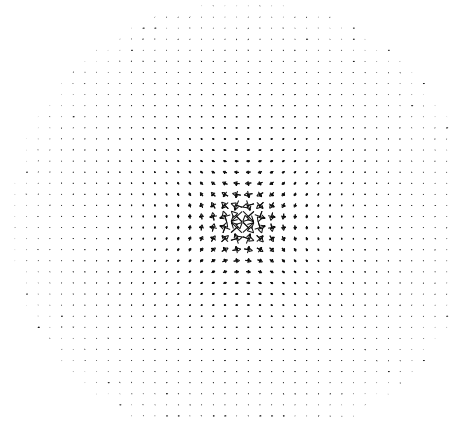
FIG. 5. The heavy vortex critical fields, below which heavy vortices become unstable, as a function of the anisotropy parameter, λ . The solid curve is the result of the variational calculation [Eq. (15)]. Data points are results of numerical energy minimization for lattice systems with radius $R = 100a$. The inset shows the asymptotic behavior at $\lambda \rightarrow 1$ more clearly.



$m = -1$, $h = 0.95$, $\omega/JS = 0.01255$

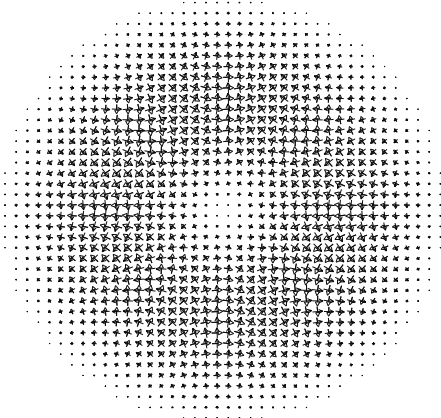


$m = -1$, $h = 0.0$, $\omega/JS = 0.002858$

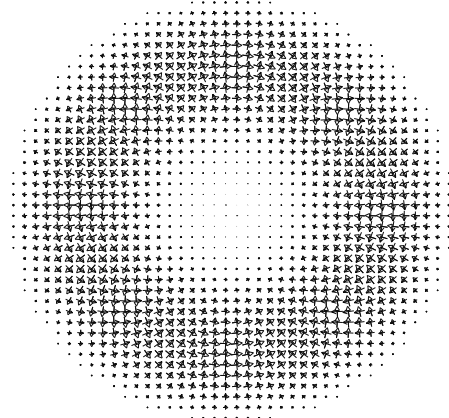


$m = -1$, $h = -0.6$, $\omega/JS = 0.0009728$

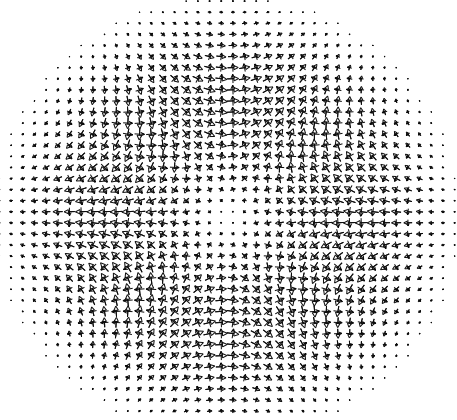
FIG. 6. Wavefunctions for $R = 20a$, $\lambda = 0.99$, for the mode with $m = -1$, at the indicated magnetic fields h . The $S^{\hat{x}}$ (or $\varphi_{\mathbf{n}}$) amplitudes (certain magnitude and phase) are shown as arrows with triangular heads, and $S^{\hat{y}}$ (or $\theta_{\mathbf{n}}$) amplitudes are shown as arrows with v-heads.³⁴



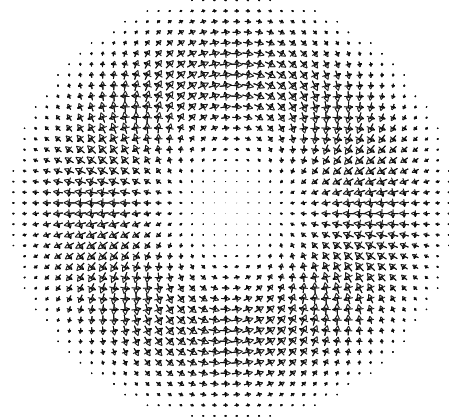
$m=-2$, $h=0.95$, $\omega/JS=0.03457$



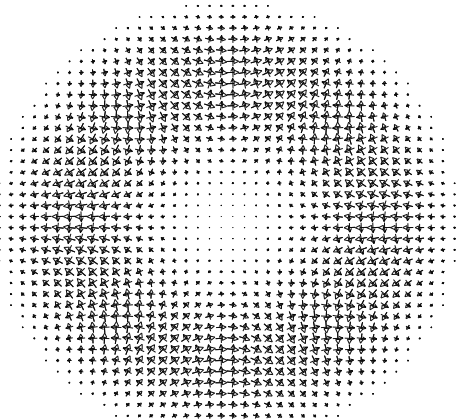
$m=+2$, $h=0.95$, $\omega/JS=0.09594$



$m=-2$, $h=0.0$, $\omega/JS=0.06454$

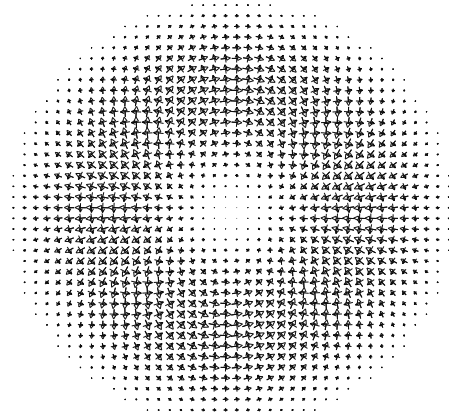


$m=+2$, $h=0.0$, $\omega/JS=0.08115$



$m=-2$, $h=-0.6$, $\omega/JS=0.09119$

FIG. 7. Wavefunctions for $R = 20a$, $\lambda = 0.99$, for the mode with $m = -2$, at the indicated magnetic fields h .



$m=+2$, $h=-0.6$, $\omega/JS=0.05602$

FIG. 8. Wavefunctions for $R = 20a$, $\lambda = 0.99$, for the mode with $m = +2$, at the indicated magnetic fields h .

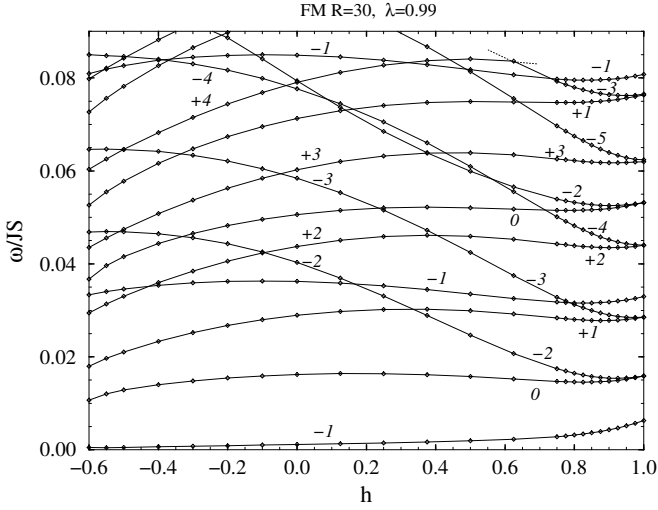


FIG. 9. Numerical results for frequencies of the lowest spin-wave modes in the presence of a light ($h > 0$) or heavy ($h < 0$) vortex in a circular system with radius $R = 30a$ and anisotropy parameter $\lambda = 0.99$, vs. the magnetic field h . Numbers by the curves indicate the assignments of azimuthal quantum numbers, m , which were based on the associated wavefunctions. Note the double degeneracies of modes $m, -(m+2)$, in the limit $h \rightarrow 1$, and the strong splitting of modes $\pm m$ as h deviates away from 0.

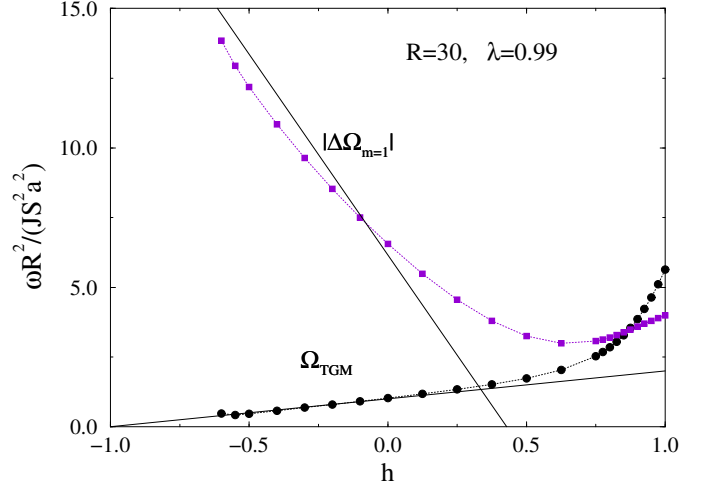


FIG. 11. Numerical results for the splitting of the lowest doublet ($n = 1$) for $|m| = 1$, and for the frequency of the translational Goldstone mode (TGM), as functions of the magnetic field h . Dashed curves are guides to the eye, while solid curves show the theoretical predictions described in the text, Eqs. (48) and (50).

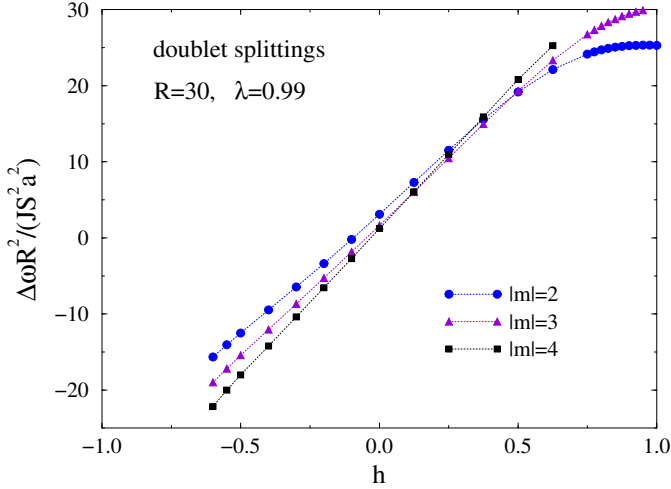


FIG. 10. Numerical results from $R = 30a$ system, for the splittings $\Delta\omega_{m,n}$ of the lowest doublets ($n = 1$) for $|m| = 2, 3, 4$, as functions of the magnetic field h . Dashed curves are guides to the eye. The slopes of the data near $h = 0$ are 29.2, 34.8, and 39.1 for $|m| = 2, 3, 4$, respectively.